



UNIVERSITY OF THE PHILIPPINES

Bachelor of Science in Physics

Janna May Z. Angeles

Cosmic evolution with interacting dark matter and dynamical dark energy

Thesis Adviser:

Michael Francis Ian G. Vega II, Ph.D.

National Institute of Physics

University of the Philippines Diliman

Date of Submission:

June 2020

Thesis Classification:

F

This thesis is available to the public

To my past, present and future self who still has very much to learn...

Acknowledgments

I would like to acknowledge the help of the following..

Sir Ian Vega for guiding and instructing me with patience and understanding and being my mentor, not only in Physics, but in life..

My fellow members in the Gravity Group for their very helpful insights and the sense of camaraderie that made me feel at home in the lab ..

My fellow batchmates, friends and church members who made my college days meaningful, fun and a bit more bearable..

DOST-SEI Merit Scholarship for making my undergraduate studies possible..

My family who served as my inspiration for their never-ending cheers, prayers and unwavering belief in me...

Thank you for all the support.

To God be the glory

ABSTRACT

COSMIC EVOLUTION WITH INTERACTING DARK MATTER AND DYNAMICAL DARK ENERGY

Janna May Z. Angeles
University of the Philippines (2020)

Adviser:
Michael Francis Ian G. Vega II,
Ph.D.

We explore the possibility that dynamic dark energy (DE) and dark matter (DM) are coupled to each other in some form of exchange (*i. e.* DM turning into DE and vice versa), and study its consequences on the late-time dynamics of a homogeneous and isotropic universe. The evolutionary equations of this model are analyzed through dynamical system methods in which fixed points of the system and their stability are determined. Phase plots of the said system were then generated to display the various behaviors of the model. We learn that for most initial states, this cosmological model ends up as a universe with a cosmological constant as its dark energy. In special cases, it may end up in various fixed points labeled by C_{\pm} , D_{\pm} , E_{\pm} , F_{\pm} , G_{\pm} , or H_{\pm} which represent universes of various curvature with varying proportions of dark matter and dynamic dark energy. In the absence of dark matter, we find that this universe with a positive curvature may not evolve towards the previously mentioned end states but towards an end state of infinitely increasing dynamic dark energy. In addition, we have also learned that the behavior of the said universe with no dark matter component can be analogous to a mechanical system as long as the Hubble parameter is constant.

PACS: 98.80.-k (Cosmology), 05.45.-a (Nonlinear dynamical systems)

Table of Contents

| | |
|---|------------|
| Acknowledgments | ii |
| Abstract | iii |
| List of Figures | v |
| List of Tables | v |
| 1 Introduction | 1 |
| 1.1 Dark matter and dark energy | 1 |
| 1.2 The Λ CDM model on DM and DE | 2 |
| 1.3 Cosmological models through dynamical systems | 2 |
| 1.4 Problem statement and overview | 3 |
| 2 Dynamical systems approach | 4 |
| 2.1 Preliminaries | 4 |
| 2.2 Linear stability analysis | 5 |
| 2.3 Classification of fixed points | 7 |
| 3 Homogenous and isotropic universes | 10 |
| 3.1 Robertson-Walker metric | 10 |
| 3.2 Friedmann equations and energy conservation law | 11 |
| 3.3 Related parameters | 12 |
| 4 Coupling of dark matter and non-dynamic dark energy | 15 |
| 4.1 The dynamical system of Ω_{dm} and Ω_{de} | 15 |
| 4.2 Stability analysis of the system | 20 |
| 4.3 Behavior of the system; phase plots | 21 |
| 5 Coupling with dark matter and dynamic dark energy | 24 |
| 5.1 The dynamical system of x , y , and s | 24 |
| 5.2 Stability analysis of the system | 32 |
| 5.3 Cosmological parameters of the fixed points | 35 |
| 5.4 System behavior and phase plots | 36 |
| 5.5 Analysis on the plane of $s = 0$ | 46 |
| 6 Conclusions and Recommendations | 52 |

List of Figures

| | | |
|-----|---|----|
| 2.1 | Stability of fixed points in a 2D phase plot | 8 |
| 2.2 | Stability of fixed points in a 3D phase plot | 9 |
| 3.1 | Types of Curvature | 11 |
| 4.1 | Phase plots of system (4.30) with $w_{\text{de}} = -1$ for different values of ϵ . (Note that other values of $w_{\text{dm}} < -1/3$ will not give any additional information. Thus, only cases of different ϵ were shown.) The solid black line pertains to $\Omega_{\text{dm}} + \Omega_{\text{de}} = 1$ | 23 |
| 4.2 | Evolution of cosmological parameters Ω_{dm} , Ω_{de} , Ω_K with respect to N for the blue trajectory in Figure 4.1b | 23 |
| 5.1 | $\{\lambda, \epsilon\}$ parameter space indicating the stability of certain fixed points . | 34 |
| 5.2 | A phase plot of system (5.40) with $\lambda = 1.2$ and $\epsilon = 1.9$ with sample trajectories in gray | 38 |
| 5.3 | $\{\lambda, \epsilon\}$ parameter space indicating the classification of phase plots . | 39 |
| 5.4 | Quadrants of the considered phase plots in the negative x region with sandy brown, blue violet, steel blue, and forest green trajectories to represent the different qualitative trajectories in this region. Point A is an unstable node in all these cases | 40 |
| 5.5 | Quadrants of the considered phase plots in the positive x region for the first case. The qualitatively different curves are represented in purple, cyan, blue, red, yellow green, yellow, orange red, magenta, pink, sea green, teal, chartreuse, turquoise, deep pink, indian red, and royal blue. | 41 |
| 5.6 | Quadrants of the considered phase plots in the positive x region for the second case. The qualitatively different curves are represented in dark red, dark orange, dark green, dark blue, gold, brown, saddle brown, red violet, dark magenta and navy blue. | 43 |
| 5.7 | Quadrants of the considered phase plots in the positive x region for the third case. The qualitatively different curves are represented in saddle brown, indigo, crimson, orange, light sea green, dark magenta, navy blue, dark slate blue, and dark olive green. | 44 |
| 5.8 | Evolution of cosmological parameters Ω_ϕ , Ω_{dm} , Ω_K , w_ϕ , and w_{tot} with respect to N for the cyan trajectory in Figure 5.5a | 45 |
| 5.9 | Evolution of cosmological parameters Ω_ϕ , Ω_{dm} , Ω_K , w_ϕ , and w_{tot} with respect to N for the saddle brown trajectory in Figure 5.7a | 46 |

| | | |
|------|--|----|
| 5.10 | Phase plots of system (5.46). The solid black curve represents $x^2 + y^2 = 1$. | 48 |
| 5.11 | A larger phase space of Figure 5.10b | 49 |
| 5.12 | Evolution of cosmological parameters Ω_ϕ , Ω_K and w_ϕ with respect to N for the dark brown trajectory in Figure 5.10b | 49 |
| 5.13 | The full evolution of Ω_ϕ and Ω_K in Figure 5.12a | 49 |
| 5.14 | The rolling ball analogy for an exponential potential | 51 |
| 5.15 | Phase plots of system (5.47) | 51 |

List of Tables

| | | |
|-----|--|----|
| 2.1 | Eigenvalues and stability of fixed points for a 2D system | 8 |
| 2.2 | Eigenvalues and stability of fixed points for a 3D system | 9 |
| 4.1 | Fixed points of system (4.30) and their corresponding eigenvalues and stability | 21 |
| 5.1 | Existence of fixed points | 33 |
| 5.2 | Stability of fixed points | 34 |
| 5.3 | Cosmological parameters of fixed points where we let $\delta = \epsilon(-6 + \lambda^2)$ and $\Delta = \sqrt{(-3 + \epsilon)(-3\lambda^2 + \epsilon(-12 + \lambda^2))}$ | 35 |
| 5.4 | Existence of fixed points for system (5.45) | 47 |
| 5.5 | Stability of fixed points | 47 |

Chapter 1

Introduction

Modern cosmology has come a long way since it began to take shape when Edwin Hubble obtained observational evidence of the Universe's expansion in 1929 [16]. Various technological advances have improved the capability of experimentalists to test the predictions of equally progressing theories in cosmology [16]. Due to this, we now have the Λ CDM model as the current standard model in this field. As the standard model in cosmology, it simulates a flat universe comprising of radiation (photons and neutrinos), ordinary (baryonic) matter, cold (non-relativistic) dark matter and the cosmological constant Λ (dark energy) [26]. So far, the model's predictions are fairly good approximations in comparison with observational data [11, 16]. Still, it does have its limitations and there are cosmological mysteries it cannot shed light on like the true nature of our Universe's dark sector.

1.1 Dark matter and dark energy

Called as "dark" because it cannot be directly observed due to the absence of interaction with electromagnetic waves, the sector is composed of dark matter (DM) and dark energy (DE) [26]. As these components are unseen, we can only detect them through their indirect influence to the visible contents of our Universe [26]. For instance, DM compensates for the missing mass in galaxies and galaxy clusters since the gravitational attraction from ordinary matter is not enough to keep these structures together. Zwicky [1] was the first to suggest this idea with compelling evidence when he measured the velocities of galaxies in the Coma cluster and inferred that the density of dark matter should be much greater than that of ordinary matter from the resulting velocity dispersion. With regards to galaxy

clusters, studies of two colliding clusters by Clowe and his peers [9, 10] have made very conclusive claims on the existence of DM with the help of gravitational lensing. [16, 26]. Another evidence of its existence is through the rotational curves of galaxies whose behavior cannot be predicted by the presence of ordinary matter alone as observed by Rubin et. al.[25].

On the other hand, the existence of dark energy, which supposedly plays a central role in the acceleration of the Universe's expansion [16, 26], can be accounted through the discrepancy on the measurement of the age of the universe in the absence of dark energy as stated by Amendola and Tsujikawa [17]. They have also stated redshift measurement from supernova observations as evidence since these measurements indicate late-time cosmic acceleration. These are supplemented by the works of Reiss et. al. [22] and the Supernova Cosmology Project [12].

1.2 The Λ CDM model on DM and DE

Although the Λ CDM model do account for the existence of these dark components, it does not give a fundamental theory regarding their behaviour and evolution. In addition, the model raises some problems like the cosmological constant and coincidence problems. The former arose from the discrepancy between the observed and theoretical value of the cosmological constant Λ [32] while the latter do so from the densities of ordinary and dark matter and dark energy which approximately coincide despite evolving differently as the Universe expands [33]. These problems motivate modifications on the standard model. Some proposed solutions include replacing Λ with dynamic dark energy in the form of a scalar field ϕ with a given potential $V(\phi)$ [2, 24], introducing a coupling between DM and DE through an arbitrary interaction term Q [3, 20] or a combination of both [4, 6, 18, 19].

1.3 Cosmological models through dynamical systems

In investigating models with such features or any cosmological models in general, dynamical systems theory is usually a useful approach [5, 30] which involves deriving mathematical expressions, typically in the form of ordinary differential equations, that describe the temporal evolution of the state variables and treating these expressions as a dynamical system [28]. By doing so, the behaviour of the

solutions for these expressions can be obtained without directly solving them [28]. Going back to the context of cosmological models, this is an advantageous feature as we can acquire qualitative information on the universe that a model depicts without directly solving the necessary equations or applying assumptions that can lead to loss of generality.

1.4 Problem statement and overview

In this thesis, we construct a model representing a homogeneous and isotropic universe in which dark matter and dynamical dark energy are coupled, and aim to understand its late-time dynamics with the use of dynamical systems. With regards to the said objective, the present work is structured as follows: we will first expand on method of dynamical systems in Chapter 2. We will then briefly discuss homogeneous and isotropic universes in Chapter 3, after which we will tackle a cosmological model with a two-dimensional dynamical system in Chapter 4 to serve as an example for the approach discussed in Chapter 2 before applying it on the more complicated system in Chapter 5 that would be the focus of this thesis. We then state the conclusions and recommendations of our discussion.

Chapter 2

Dynamical systems approach

Cosmological models are often characterized by nonlinear systems which can be hard to solve and interpret. As mentioned in the previous chapter, the dynamical system approach can be an advantageous method in analyzing such models since we no longer have to solve for exact solutions in order to understand the model's behavior. In this chapter, we discuss aspects of dynamical systems that we shall use in our later analysis of our cosmological models. For a complete discussion on this topic, we direct you to [5, 23, 28] where much of our discussion of the subject matter come from.

2.1 Preliminaries

Before we get into the details, it is convenient to introduce a few terms that we frequently use throughout the thesis:

- **Dynamical system** - Simply put, this is a system which shows how state variables evolve as time passes. Ordinary differential equations (ODEs) are the most common forms of dynamical system and can be treated as a vector field.
- **State variables** - These are the variables that contain the bits of information needed to determine the state of the system and predict future states.
- **State** - This is a description of the system.
- **Trajectory** - This is a visualization of a function that is a solution to

the equations in the system. In other words, it represents the system's evolution from an initial condition.

- Fixed point - This represents an equilibrium solution in which the state variables' rates of change become zero. A trajectory with a fixed point as its initial condition will stay on that point.
- Stability - This is a qualitative measure on how trajectories behave in relation to a fixed point.
- Jacobian matrix - This is a matrix that has first-order partial derivatives of the differential equations with respect to the state variables as its elements.
- Phase space - This space is a graphical representation of the system with state variables as coordinates in it.
- Phase plot - This is a region in the phase space that shows the qualitatively different trajectories and fixed points the system have.
- Invariant manifold - This is a subspace in the phase space where trajectories in this subspace evolve without leaving its boundaries.

We can move on to the method of characterizing fixed points with their stability. Since fixed points dominate the analysis and interpretation of phase plots, characterizing fixed points is important when applying dynamical systems. The stability of a fixed point can be inferred from the behaviour of nearby trajectories which we can usually obtain from linear stability analysis.

2.2 Linear stability analysis

Let us consider a set of ordinary differential equations in the form

$$\begin{aligned}\dot{x}_1 &= f_1(x_1, \dots, x_n) \\ &\vdots \\ \dot{x}_n &= f_n(x_1, \dots, x_n)\end{aligned}\tag{2.1}$$

as our dynamical system with state variables $\{x_1, \dots, x_n\}$. Here, $\dot{x}_j = dx_j/dt$ where $j = 1, \dots, n$. Assuming that the equations are independent from each other, Eq.

(2.1) is an n -dimensional or n th-order system and the solutions of these equations can be graphically represented as trajectories flowing in an n -dimensional phase space. Notice that the functions f_1, \dots, f_n are autonomous (*i.e.* no explicit time-dependence) so this phase space does not contain any time information. The said set of equations can be written in a more compact expression as a vector field

$$\dot{\mathbf{x}} = \mathbf{f}(\mathbf{x}) \quad (2.2)$$

where $\mathbf{x} = (x_1, \dots, x_n)$ and $\mathbf{f}(\mathbf{x}) = (f_1(\mathbf{x}), \dots, f_n(\mathbf{x}))$. Note that \mathbf{x} is a point in phase space and $\dot{\mathbf{x}}$ is the vector at that point.

Supposing that $\mathbf{x}^* = (x_1^*, \dots, x_n^*)$ is a fixed point for it satisfies $\mathbf{f}(\mathbf{x}^*) = 0$, we can characterize this point by its stability. We do this by letting some small displacement from the fixed point be defined as $\delta\mathbf{x} = \mathbf{x} - \mathbf{x}^*$. The vector at this displacement is given by $\dot{\delta\mathbf{x}} = \dot{\mathbf{x}}$ since \mathbf{x}^* is just a constant. Taking the multivariate Taylor expansion of $\mathbf{f}(\mathbf{x})$ at \mathbf{x}^* ,

$$\dot{\mathbf{x}} = \underbrace{\mathbf{f}(\mathbf{x}^*)}_{0} + \frac{1}{1!} \left. \frac{\partial \mathbf{f}}{\partial \mathbf{x}} \right|_{\mathbf{x}=\mathbf{x}^*} (\mathbf{x} - \mathbf{x}^*) + \dots \quad (2.3)$$

$$\dot{\delta\mathbf{x}} = \left. \frac{\partial \mathbf{f}}{\partial \mathbf{x}} \right|_{\mathbf{x}=\mathbf{x}^*} \delta\mathbf{x} + \dots \quad (2.4)$$

From the given definition of the Jacobian matrix, we know that

$$\left. \frac{\partial \mathbf{f}}{\partial \mathbf{x}} \right|_{\mathbf{x}=\mathbf{x}^*} = \begin{pmatrix} \frac{\partial f_1}{\partial x_1} & \dots & \frac{\partial f_1}{\partial x_n} \\ \vdots & \ddots & \vdots \\ \frac{\partial f_n}{\partial x_1} & \dots & \frac{\partial f_n}{\partial x_n} \end{pmatrix}_{(x_1^*, \dots, x_n^*)} \equiv J^* \quad (2.5)$$

where J^* is the Jacobian matrix evaluated at \mathbf{x}^* . Also, notice that higher order terms of the already small $\delta\mathbf{x}$ are so tiny that they usually become negligible. With those in mind, Eq. (2.4) can be turned to a linearized system expressed as

$$\dot{\delta\mathbf{x}} = J^* \delta\mathbf{x} \quad (2.6)$$

Since this is a linearized system, we can now apply linear algebra methods which state that the solutions of Eq. (2.6) can be written as a linear combination of terms in the form $e^{\lambda_j t} \mathbf{v}_j$ where $\{\lambda_j\}$ and $\{\mathbf{v}_j\}$ are the set of eigenvalues and eigenvectors of the Jacobian matrix J^* . Therefore, trajectories near the fixed point approximately evolves as some combination of various exponential motion directed by eigenvectors as expressed by

$$\delta\mathbf{x}(t) = e^{\lambda_1 t} \mathbf{v}_1 + \dots + e^{\lambda_n t} \mathbf{v}_n \quad (2.7)$$

assuming that the eigenvalues are distinct which means that their corresponding eigenvectors are linearly independent and span the whole phase space. Notice that if the elements of $\{\lambda_j\}$ are all negative [positive] and real, then $\delta x(t)$ shrinks [grows] as time passes which means trajectories will tend to move toward [away from] the fixed point. This is also somewhat applicable for the general case of complex eigenvalues, which occur as complex conjugate pairs, as we see in the following expression with the use of Euler's formula:

$$e^{\lambda_j t} = e^{(\alpha_j + i\omega_j)t} = e^{\alpha_j t} e^{i\omega_j t} = e^{\alpha_j t} (\cos \omega_j + i \sin \omega_j) \quad (2.8)$$

The imaginary part just contributes an oscillating behaviour to the trajectories which indicates that the real part decides whether they move toward or away from the fixed point. We see here that it is the eigenvalues, specifically the signs of their real part, that determines the stability of fixed points and we will use this in classifying them in the next section.

We want to note, however, that there are cases where this analysis falls apart. For instance, the fixed point could have purely imaginary eigenvalues. Going back at Eq. (2.8), we can infer that the behavior of nearby trajectories become completely oscillatory around this point. Since their real parts are non-existent, we cannot determine its stability. Other cases would be that the fixed point could have a zero eigenvalue or an indeterminate Jacobian matrix when evaluated at this point. For these instances, we can usually look into the system's phase plot to get an idea of the point's stability.

2.3 Classification of fixed points

With eigenvalues playing a central role in analyzing stability, it is only natural to classify fixed points based on the nature of their corresponding eigenvalues. In Table 2.1, we list down the possible kinds of fixed points for a two-dimensional system which are graphically shown in Figure 2.1 [21]. We do the same for a three-dimensional system in Table 2.2 and Figure 2.2 [15]. We have also included the case of a fixed point with purely imaginary eigenvalues for our reference.

Now that we have an idea in using dynamical systems, we finally have a picture of how our analysis of our cosmological models will proceed. Before we do that, however, we will first lay down some more terminology and equations, this time in

relation to homogeneous and isotropic universes as these are essentially the building blocks of our models.

Table 2.1: Eigenvalues and stability of fixed points for a 2D system

| Eigenvalues | Fixed Point |
|---|---|
| $\text{Im}(\lambda_{1,2}) = 0, \lambda_{1,2} < 0$ | stable node: trajectories are attracted to the fixed point |
| $\text{Im}(\lambda_{1,2}) = 0, \lambda_{1,2} > 0$ | unstable node: trajectories are repelled away from the fixed point |
| $\text{Im}(\lambda_{1,2}) = 0, \lambda_1 > 0, \lambda_2 < 0$ | saddle: some trajectories are attracted to the fixed point while some are repelled away |
| $\text{Im}(\lambda_{1,2}) \neq 0, \text{Re}(\lambda_{1,2}) < 0$ | stable focus/spiral: trajectories spiral towards the fixed point |
| $\text{Im}(\lambda_{1,2}) \neq 0, \text{Re}(\lambda_{1,2}) > 0$ | unstable focus/spiral: trajectories spiral away from the fixed point |
| $\text{Im}(\lambda_{1,2}) \neq 0, \text{Re}(\lambda_{1,2}) = 0$ | center: trajectories are neither attracted to or repelled away from the fixed point and form closed orbits around it |

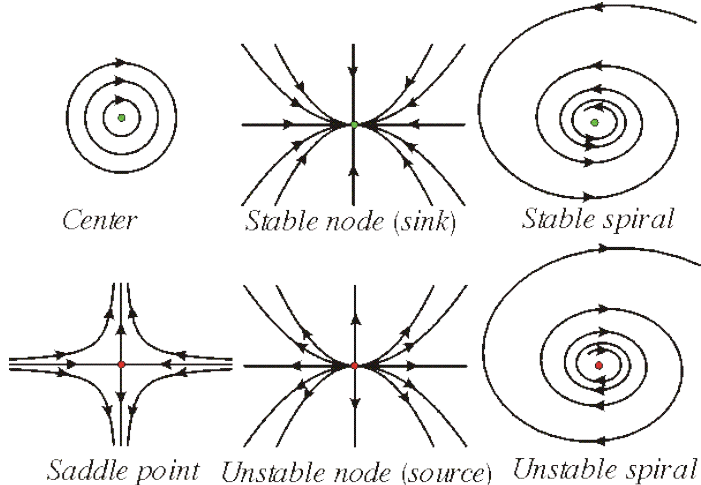


Figure 2.1: Stability of fixed points in a 2D phase plot

Table 2.2: Eigenvalues and stability of fixed points for a 3D system

| Eigenvalues | Fixed Point |
|--|--|
| $\text{Im}(\lambda_{1,2,3}) = 0, \lambda_{1,2,3} < 0$ | stable node: trajectories are attracted to the fixed point |
| $\text{Im}(\lambda_{1,2,3}) = 0, \lambda_{1,2,3} > 0$ | unstable node: trajectories are repelled away from the fixed point |
| $\text{Im}(\lambda_{1,2,3}) = 0, \lambda_1 < \lambda_2 < 0 < \lambda_3$ or $\lambda_1 < 0 < \lambda_2 < \lambda_3$ | saddle: some trajectories are attracted to the fixed point while some are repelled away |
| $\text{Im}(\lambda_{1,2}) \neq 0$ and $\text{Im}(\lambda_3) = 0$, $\text{Re}(\lambda_{1,2}) < 0$ and $\lambda_3 < 0$ | stable focus/spiral-node: some trajectories spiral towards the fixed point |
| $\text{Im}(\lambda_{1,2}) \neq 0$ and $\text{Im}(\lambda_3) = 0$, $\text{Re}(\lambda_{1,2}) > 0$ and $\lambda_3 > 0$ | unstable focus/spiral-node: some trajectories spiral away from the fixed point |
| $\text{Im}(\lambda_{1,2}) \neq 0$ and $\text{Im}(\lambda_3) = 0$, $\text{Re}(\lambda_{1,2}) < [>] 0$ and $\lambda_3 > [<] 0$ | saddle focus/spiral-node: some trajectories spiral away from [towards] the fixed point while some are attracted to [repelled from] it |
| $\text{Im}(\lambda_{1,2,3}) \neq 0, \text{Re}(\lambda_{1,2,3}) = 0$ | center: trajectories are neither attracted to or repelled away from the fixed point and form closed orbits around it |

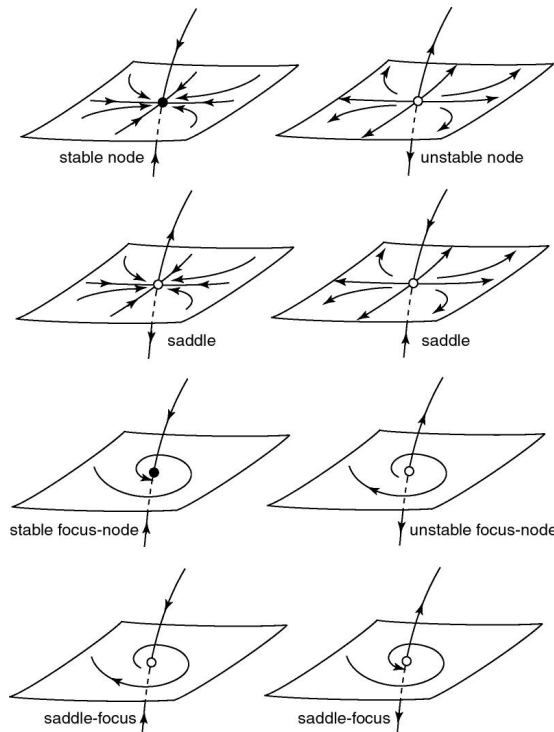


Figure 2.2: Stability of fixed points in a 3D phase plot

Chapter 3

Homogenous and isotropic universes

Our cosmological models are homogeneous and isotropic. This means that they simulate a universe which looks the same in every direction (isotropy) and at every location (homogeneity). This is the cosmological principle. We set our models in this way because our Universe follows this principle when we observe it over large scales. Also, applying this principle often simplifies calculations on our models. In this chapter, we continue to define and introduce concepts that would help in constructing and understanding the cosmological models in the next chapters. An in-depth discourse on this topic can be found in [7, 26, 29]; our discussion borrows heavily from these references.

3.1 Robertson-Walker metric

We define a metric as a mathematical expression that gives a sense of distance in an arbitrary space. Since Euclidean geometry is no longer enough to measure distances in our vast Universe where space and time are intricately linked together, we need a metric to do so. For homogeneous and isotropic universes, distances are generally defined by the Robertson-Walker metric expressed as

$$ds^2 = -c^2 dt^2 + a^2(t) \left[\frac{dr^2}{1 - Kr^2} + r^2 (d\theta^2 + \sin^2 \theta d\phi^2) \right] \quad (3.1)$$

where K is a curvature parameter and $a(t)$ is a dimensionless scale factor that describes how such a universe expands or contracts with time. This metric contains three spatial geometries that the universe can possess. It can either be flat ($K = 0$), spatially-closed ($K > 0$), or spatially-open ($K < 0$) which are graphically shown in Figure 3.1 (modified from [26]).

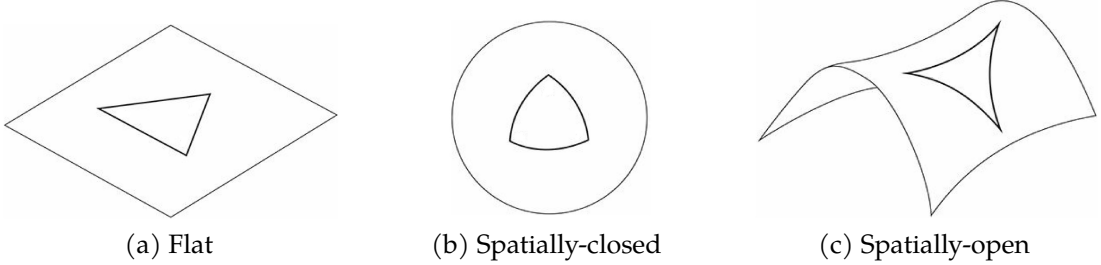


Figure 3.1: Types of Curvature

3.2 Friedmann equations and energy conservation law

Now, bear in mind that a perfect fluid is characterized only by its energy density $\rho(t)$ and isotropic pressure $P(t)$ which are related by an equation of state (EoS), often in the form of

$$P = w\rho c^2 \quad (3.2)$$

where the EoS parameter w is dimensionless. Assuming that the components of this universe behave like a perfect fluid, we plug the said metric into Einstein's field equations which govern the universe's evolution. These then take the form of the Friedmann equations written as

$$\left(\frac{\dot{a}}{a}\right)^2 = \frac{\kappa^2}{3}\rho - \frac{Kc^2}{a^2} \quad (3.3)$$

$$\frac{\ddot{a}}{a} = -\frac{\kappa^2}{6}\left(\rho + 3\frac{P}{c^2}\right) \quad (3.4)$$

where $\kappa^2 = 8\pi G$. The first Friedmann equation relates the components of the universe with its curvature. From the second one, we can get an idea on whether its expansion or contraction is accelerating ($\ddot{a} > 0$) or decelerating ($\ddot{a} < 0$). Another resulting equation is

$$\dot{\rho} = -3\frac{\dot{a}}{a}\left(\rho + \frac{P}{c^2}\right) \quad (3.5)$$

which is an expression of energy conservation. These are the key equations that determine how the scale factor $a(t)$ of the universe behaves and evolves with time in relation with the various components of the universe. Note that Eqs. (3.3), (3.4) and (3.5) may be written for a single energy density but this is not the case in reality so they are usually written for a combination of different energy densities, each with their own equation of state. Also, we will express these equations in geometric units (*i.e.* $G = 1, c = 1$) from now on for easier calculation and tracking of terms.

Let's sidetrack for a little from the main discussion to talk about the behavior of DM and DE in the context of their EoS parameters. For DM, it is pretty straightforward. We will assume that it is non-relativistic and pressureless [27] so we let its corresponding EoS parameter to be $w_{\text{dm}} = 0$. As for DE, there is the cosmological constant which is a special type of the said component. In terms of energy density, it can be expressed as $\rho_{\Lambda} = c^2 \Lambda / \kappa^2$ with a corresponding EoS parameter of $w_{\Lambda} = -1$. In general, the EoS parameter for dark energy falls in the range of $w_{\text{de}} < -1/3$ since this is the condition to achieve accelerated expansion. We see this in Eq. (3.6) where we substituted the equation of state into Eq. (3.4) and factored out ρ_{de} .

$$\frac{\ddot{a}}{a} = -\frac{\kappa^2}{6} (1 + 3w_{\text{de}}) \rho_{\text{de}} \quad (3.6)$$

3.3 Related parameters

To transform Eqs. (3.3) and (3.5) so that they will be more usable when constructing dynamical systems in the following chapters, we can express them in terms of some quantities we shall introduce in this section. One such quantity is the Hubble parameter

$$H = \frac{\dot{a}}{a} \quad (3.7)$$

which characterizes the rate of expansion of the universe. Another quantity, measures the acceleration of the expansion, is the dimensionless deceleration parameter given by

$$q = -\frac{\ddot{a}a}{\dot{a}^2} = -\frac{\ddot{a}}{aH^2} \quad (3.8)$$

Regarding these two parameters, it would be convenient later on to derive from taking the time derivative of the Hubble parameter in Eq. (3.7)

$$\dot{H} = \frac{a\ddot{a} - \dot{a}\dot{a}}{a^2} = \frac{\alpha\ddot{a}}{a^2} - \left(\frac{\dot{a}}{a}\right)^2 = \frac{\ddot{a}}{a} - H^2 \quad (3.9)$$

that

$$\frac{\dot{H}}{H^2} = \frac{\ddot{a}}{aH^2} - 1 = -\left(1 - \frac{\ddot{a}}{aH^2}\right) \quad (3.10)$$

Thus, using Eq. (3.8), we have

$$\frac{\dot{H}}{H^2} = -(1 + q) \quad (3.11)$$

There are also the density parameters defined as

$$\Omega \equiv \frac{\kappa\rho}{3H^2} \quad (3.12)$$

$$\Omega_K \equiv -\frac{K}{a^2 H^2} \quad (3.13)$$

which are dimensionless quantities pertaining to relative abundances of the content and curvature in the universe. In terms of these parameters, Eq. (3.3) can be written as

$$1 = \Omega + \Omega_K \quad (3.14)$$

Thus, the curvature will depend on the value of Ω as follows:

$$\begin{aligned} \Omega < 1 &\rightarrow \Omega_K > 0 \rightarrow K < 0 \\ \Omega = 1 &\rightarrow \Omega_K = 0 \rightarrow K = 0 \\ \Omega > 1 &\rightarrow \Omega_K < 0 \rightarrow K > 0. \end{aligned} \quad (3.15)$$

We also introduce a time parameter $N = \ln a$ where N is called the number of e -foldings. An e -folding is a measure of how much the scale factor increases by a factor of e [31]. Note that the derivative of any quantity X with respect to N , which we shall denote by its prime derivative X' , is related to its time derivative \dot{X} by

$$\begin{aligned} \frac{dX}{dt} &= \frac{dX}{dN} \frac{dN}{dt} \\ \dot{X} &= X' \frac{d \ln a}{dt} \\ &= X' \frac{\dot{a}}{a} \\ \dot{X} &= X' H \end{aligned} \quad (3.16)$$

Thus, we have

$$X' = \frac{\dot{X}}{H} \quad (3.17)$$

Equivalently, we have $dN = H dt$. Using this, the prime derivative of the scale factor is

$$a' = \frac{\dot{a}}{H} = \dot{a} \cdot \frac{a}{\dot{a}} = a \quad (3.18)$$

and the relation in Eq. (3.11) becomes

$$\frac{\dot{H}}{H} \frac{1}{H} = -(1 + q) \longrightarrow H' = -(1 + q)H \quad (3.19)$$

Following convention, we shall use N instead of t for the cosmological models in this thesis because it is dimensionless and contracts a vast amount of time (about billions

of years) into a shorter but equivalent time scale. Furthermore, we will find out in later chapters that choosing N can make our dynamical system H -independent, which can simplify our analysis.

With these concepts tackled, we can now construct homogeneous and isotropic cosmological models with various components. Discussing the behavior and evolution arising from such models is our next step. A good start would be a model where dark matter is coupled with non-dynamic dark energy as we will examine in the next chapter.

Chapter 4

Coupling of dark matter and non-dynamic dark energy

In their paper, Perez et. al. [20] studied a cosmological model where dark matter and non-dynamic dark energy interact with each other in a non-flat, homogeneous, and isotropic universe. In this chapter, we will revisit this model. The purpose of this chapter is twofold: it serves as a testbed example for the use of the methods discussed in Chapter 2 and, at the same time, introduces a less complicated model with similar enough characteristics to ease our discussion for the model in Chapter 5.

4.1 The dynamical system of Ω_{dm} and Ω_{de}

For this cosmological scenario, we shall consider a non-flat, homogeneous, and isotropic universe composed only of dark matter and dark energy. With these considerations, we can express Eq. (3.3) as

$$\left(\frac{\dot{a}}{a}\right)^2 = \frac{\kappa^2}{3} (\rho_{\text{de}} + \rho_{\text{dm}}) - \frac{K}{a^2} \quad (4.1)$$

and Eq. (3.4) into

$$\frac{\ddot{a}}{a} = -\frac{\kappa^2}{6} ((\rho_{\text{de}} + \rho_{\text{dm}}) + 3(P_{\text{de}} + P_{\text{dm}})) \quad (4.2)$$

Note that Eq. (4.1) can be rearranged into

$$1 = \frac{\kappa^2}{3H^2} \rho_{\text{de}} + \frac{\kappa^2}{3H^2} \rho_{\text{dm}} - \frac{K}{a^2 H^2} \quad (4.3)$$

by dividing the whole equation by H^2 which becomes

$$1 = \Omega_{\text{de}} + \Omega_{\text{dm}} + \Omega_K \quad (4.4)$$

with the use of density parameters given in the previous chapter where

$$\Omega_{\text{de}} = \frac{\kappa^2}{3H^2}\rho_{\text{de}}, \quad \Omega_{\text{dm}} = \frac{\kappa^2}{3H^2}\rho_{\text{dm}} \quad (4.5)$$

Now, let us calculate the deceleration parameter for this cosmology. Recall the definition of q in Eq. (3.8). Note that from Eq. (4.1), we have

$$\ddot{a}^2 = a^2 \left(\frac{\kappa^2}{3}\rho_{\text{de}} + \frac{\kappa^2}{3}\rho_{\text{dm}} - \frac{K}{a^2 H^2} \right) \quad (4.6)$$

Also, rearranging Eq. (4.2) gives

$$\ddot{a} = a \left[-\frac{\kappa^2}{6} ((\rho_{\text{de}} + \rho_{\text{dm}}) + 3(P_{\text{de}} + P_{\text{dm}})) \right] \quad (4.7)$$

Thus, q is now

$$\begin{aligned} q &= -\frac{\ddot{a}a}{\dot{a}^2} \\ &= -\frac{\alpha \left[-\frac{\kappa^2}{6} ((\rho_{\text{de}} + \rho_{\text{dm}}) + 3(P_{\text{de}} + P_{\text{dm}})) \right] \cdot \alpha}{\alpha^2 \left(\frac{\kappa^2}{3}\rho_{\text{de}} + \frac{\kappa^2}{3}\rho_{\text{dm}} - \frac{Kc^2}{a^2} \right)} \\ q &= -\left(-\frac{1}{2} \right) \frac{\frac{\kappa^2}{3}\rho_{\text{de}} + \frac{\kappa^2}{3}\rho_{\text{dm}} + \kappa^2 P_{\text{de}} + \kappa^2 P_{\text{dm}}}{H^2} \end{aligned} \quad (4.8)$$

from Eq. (4.1) with the definition of the Hubble parameter in Eq. (3.7). Using the given EoS in Eq. (3.2) to express the pressure in terms of the energy density and substituting the density parameters, we have

$$\begin{aligned} q &= \frac{1}{2} \frac{\frac{\kappa^2}{3}\rho_{\text{de}} + \frac{\kappa^2}{3}\rho_{\text{dm}} + \kappa^2 w_{\text{de}}\rho_{\text{de}} + \kappa^2 w_{\text{dm}}\rho_{\text{dm}}}{H^2} \\ &= \frac{1}{2} \frac{\Omega_{\text{de}}H^2 + \Omega_{\text{dm}}H^2 + 3w_{\text{de}}\Omega_{\text{de}}H^2 + 3w_{\text{dm}}\Omega_{\text{dm}}H^2}{H^2} \\ &= \frac{1}{2} (\Omega_{\text{de}} + \Omega_{\text{dm}} + 3w_{\text{de}}\Omega_{\text{de}} + 3w_{\text{dm}}\Omega_{\text{dm}}) \\ q &= \frac{1}{2} [(1 + 3w_{\text{de}})\Omega_{\text{de}} + (1 + 3w_{\text{dm}})\Omega_{\text{dm}}] \end{aligned} \quad (4.9)$$

Recall that we let $w_{\text{dm}} = 0$ which turns (4.9) into

$$q = \frac{1}{2} [(1 + 3w_{\text{de}})\Omega_{\text{de}} + \Omega_{\text{dm}}] \quad (4.10)$$

As for the coupling between DM and DE, this can be mathematically expressed by

$$\dot{\rho}_{\text{de}} + 3H(\rho_{\text{de}} + P_{\text{de}}) = -Q \quad (4.11)$$

$$\dot{\rho}_{\text{dm}} + 3H(\rho_{\text{dm}} + P_{\text{dm}}) = Q \quad (4.12)$$

where the interaction term is given as $Q = \frac{\kappa^2}{3H}\epsilon\rho_{\text{de}}\rho_{\text{dm}}$ with ϵ as a non-negative constant. We choose this Q to relate the interaction to the abundance of the coupled components. By again applying the given EoS and factoring out the energy densities, we have

$$\dot{\rho}_{\text{de}} + 3H\rho_{\text{de}}(1+w_{\text{de}}) = -Q \quad (4.13)$$

$$\dot{\rho}_{\text{dm}} + 3H\rho_{\text{dm}} = Q \quad (4.14)$$

again with $w_{\text{dm}} = 0$. We will also constrain w_{de} to be less than $1/3$ as explained in the previous chapter. Obtaining ρ'_{dm} and ρ'_{de} would be handy when we derive our dynamical system. For the former, we substitute the interaction term into (4.14) and arrange the resulting equation to get

$$\begin{aligned} \dot{\rho}_{\text{dm}} &= -3H\rho_{\text{dm}} + \frac{\kappa^2}{3H}\epsilon\rho_{\text{de}}\rho_{\text{dm}} \\ &= H \left[-3\rho_{\text{dm}} + \frac{\kappa^2}{3H^2}\epsilon\rho_{\text{de}}\rho_{\text{dm}} \right] \end{aligned} \quad (4.15)$$

which we can express as

$$\frac{\dot{\rho}_{\text{dm}}}{H} = \rho'_{\text{dm}} = -3\rho_{\text{dm}} + \frac{\kappa^2}{3H^2}\epsilon\rho_{\text{de}}\rho_{\text{dm}} \quad (4.16)$$

by applying Eq. (3.17). In the same manner, from (4.13)

$$\begin{aligned} \dot{\rho}_{\text{de}} &= -3H\rho_{\text{de}}(1+w_{\text{de}}) - \frac{\kappa^2}{3H}\epsilon\rho_{\text{de}}\rho_{\text{dm}} \\ &= H \left[-3\rho_{\text{de}}(1+w_{\text{de}}) - \frac{\kappa^2}{3H^2}\epsilon\rho_{\text{de}}\rho_{\text{dm}} \right] \end{aligned} \quad (4.17)$$

we obtain

$$\frac{\dot{\rho}_{\text{de}}}{H} = \rho'_{\text{de}} = -3\rho_{\text{de}}(1+w_{\text{de}}) - \frac{\kappa^2}{3H^2}\epsilon\rho_{\text{de}}\rho_{\text{dm}} \quad (4.18)$$

With that done, we can now derive the differential equations that will make up our dynamical system. We start with the derivative of Ω_K with respect to N in which we have

$$\Omega'_K = \frac{d}{dN} \left(-\frac{Kc^2}{a^2H^2} \right) = -Kc^2 \frac{d}{dN} \left(\frac{1}{a^2H^2} \right) \quad (4.19)$$

Before proceeding, we note that

$$\frac{d}{dN} \left(\frac{1}{H^2} \right) = \frac{d}{dH} \left(\frac{1}{H^2} \right) \frac{dH}{dN} = -\frac{2}{H^3}H' \quad (4.20)$$

and

$$\frac{d}{dN} \left(\frac{1}{a^2} \frac{1}{H^2} \right) = \frac{1}{a^2} \frac{d}{dN} \left(\frac{1}{H^2} \right) + \frac{1}{H^2} \frac{d}{dN} \left(\frac{1}{a^2} \right) \quad (4.21)$$

Applying Eq. (4.20) and using it as an example for $\frac{d}{dN} \frac{1}{a^2}$, Eq. (4.21) becomes

$$\begin{aligned} \frac{d}{dN} \left(\frac{1}{a^2} \frac{1}{H^2} \right) &= \frac{1}{a^2} \left(-\frac{2}{H^3} H' \right) + \frac{1}{H^2} \left(-\frac{2}{a^3} a' \right) \\ &= \frac{1}{a^2} \left(-\frac{2}{H^2} [-(1+q)\mathbb{H}] \right) + \frac{1}{H^2} \left(-\frac{2}{a^2} \alpha \right) \\ \frac{d}{dN} \left(\frac{1}{a^2} \frac{1}{H^2} \right) &= \frac{2}{a^2 H^2} (\lambda + q - \lambda) \end{aligned} \quad (4.22)$$

with Eq. (3.18) and Eq. (3.19). Thus, by substituting Eq. (4.22) into Eq. (4.19), we obtain

$$\Omega'_K = -\frac{Kc^2}{a^2 H^2} 2q = 2q\Omega_K \quad (4.23)$$

As for the prime derivative of Ω_{dm} , we start with

$$\begin{aligned} \Omega'_{dm} &= \frac{d}{dN} \Omega_{dm} \\ &= \frac{d}{dN} \left(\frac{\kappa^2 \rho_{dm}}{3H^2} \right) \\ &= \frac{\kappa^2}{3} \frac{d}{dN} \left(\frac{\rho_{dm}}{H^2} \right) \\ &= \frac{\kappa^2}{3} \frac{H^2 \rho'_{dm} - \rho_{dm}(2HH')}{H^4} \\ \Omega'_{dm} &= \frac{\kappa^2}{3} \left[\frac{\rho'_{dm}}{H^2} - \frac{2\rho_{dm}(-(1+q)\mathbb{H})}{H^2} \right] \end{aligned} \quad (4.24)$$

after applying Eq. (3.19) to H' . Then, we have

$$\begin{aligned} \Omega'_{dm} &= \frac{\kappa^2}{3H^2} [\rho'_{dm} - 2\rho_{dm}(-(1+q))] \\ &= \frac{\kappa^2}{3H^2} \left[-3\rho_{dm} + \frac{\kappa^2}{3H^2} \epsilon \rho_{de} \rho_{dm} - 2\rho_{dm}(-(1+q)) \right] \end{aligned} \quad (4.25)$$

by substituting in Eq. (4.16). Factoring out ρ_{dm} , we get

$$\begin{aligned} \Omega'_{dm} &= \frac{\kappa^2 \rho_{dm}}{3H^2} \left[-3 + \frac{\kappa^2 \rho_{de}}{3H^2} \epsilon + 2 + 2q \right] \\ &= \Omega_{dm} (-1 + \Omega_{de} \epsilon + 2q) \\ &= \Omega_{dm} [-1 + \epsilon \Omega_{de} + (1 + 3w_{de}) \Omega_{de} + \Omega_{dm}] \\ \Omega'_{dm} &= \Omega_{dm} [-1 + (1 + 3w_{de} + \epsilon) \Omega_{de} + \Omega_{dm}] \end{aligned} \quad (4.26)$$

after also substituting in Eq. (4.10). In the same manner, for Ω'_{de} , we start with

$$\begin{aligned}
\Omega'_{\text{de}} &= \frac{d}{dN} \Omega_{\text{de}} \\
&= \frac{d}{dN} \left(\frac{\kappa^2 \rho_{\text{de}}}{3H^2} \right) \\
&= \frac{\kappa^2}{3} \frac{d}{dN} \left(\frac{\rho_{\text{de}}}{H^2} \right) \\
&= \frac{\kappa^2}{3} \frac{H^2 \rho'_{\text{de}} - \rho_{\text{de}}(2HH')}{H^4} \\
\Omega'_{\text{de}} &= \frac{\kappa^2}{3} \left[\frac{\rho'_{\text{de}}}{H^2} - \frac{2\rho_{\text{de}}(-(1+q)\mathcal{H})}{H^3} \right]
\end{aligned} \tag{4.27}$$

after utilizing Eq. (3.19). Then, we have

$$\begin{aligned}
\Omega'_{\text{de}} &= \frac{\kappa^2}{3H^2} [\rho'_{\text{de}} - 2\rho_{\text{de}}(-(1+q))] \\
&= \frac{\kappa^2}{3H^2} \left[-3\rho_{\text{de}}(1+w_{\text{de}}) - \frac{\kappa^2}{3H^2} \epsilon \rho_{\text{de}} \rho_{\text{dm}} - 2\rho_{\text{de}}(-(1+q)) \right]
\end{aligned} \tag{4.28}$$

by replacing ρ'_{de} with Eq. (4.18). Factoring out ρ_{de} ,

$$\begin{aligned}
\Omega'_{\text{de}} &= \frac{\kappa^2 \rho_{\text{de}}}{3H^2} \left[-3^{-1} - 3w_{\text{de}} - \frac{\kappa^2 \rho_{\text{dm}}}{3H^2} \epsilon + 2 + 2q \right] \\
&= \Omega_{\text{de}}(-1 - 3w_{\text{de}} - \Omega_{\text{dm}}\epsilon + 2q) \\
&= \Omega_{\text{de}}[-1 - 3w_{\text{de}} - \epsilon\Omega_{\text{dm}} + (1 + 3w_{\text{de}})\Omega_{\text{de}} + \Omega_{\text{dm}}] \\
\Omega'_{\text{de}} &= \Omega_{\text{de}}[-1 - 3w_{\text{de}} + (1 + 3w_{\text{de}})\Omega_{\text{de}} + (1 - \epsilon)\Omega_{\text{dm}}]
\end{aligned} \tag{4.29}$$

after also substituting in Eq. (4.10).

Along with Eq. (3.19), the system made up of Eqs. (4.19), (4.29), and (4.27) fully characterize a universe where dark matter and non-dynamic dark energy interact with each other. However, considering all of these equations as part of our dynamical system will just make our analysis complicated. There is no need to include H' because it can be determined once the said system of equations, which has no explicit H -dependence, is solved. In addition, the constraint imposed by Eq. (4.3) makes one of the equations in the system redundant. Therefore, we have

$$\begin{cases} \Omega'_{\text{dm}} = \Omega_{\text{dm}}[-1 + (1 + 3w_{\text{de}} + \epsilon)\Omega_{\text{de}} + \Omega_{\text{dm}}] \\ \Omega'_{\text{de}} = \Omega_{\text{de}}[-1 - 3w_{\text{de}} + (1 + 3w_{\text{de}})\Omega_{\text{de}} + (1 - \epsilon)\Omega_{\text{dm}}] \end{cases} \tag{4.30}$$

as our dynamical system with state variables Ω_{dm} and Ω_{de} . We note that we did not specify the scale factor in the construction of this system. This means that the behavior of system 4.30 should hold for all expressions of $a(t)$.

Before we move on, let us have brief interlude to recognize the relation of this dynamical system with the Lotka-Volterra model which is a simple interaction model that studies the population dynamics in an ecosystem with a single predator and prey species [13, 14]. As expressed by Perez et. al. [20], the Lotka-Volterra system is composed of coupled nonlinear ordinary differential equations given as

$$\begin{cases} \dot{x}_1 = x_1 (+r_1 - a_{12}x_2) \\ \dot{x}_2 = x_2 (-r_2 + a_{21}x_1) \end{cases} \quad (4.31)$$

where x_1 and x_2 are the prey and predator species respectively and r_1 [r_2] is a constant representing the growth [death] rate of the prey [predator] in the absence the other species. The constants a_{12} and a_{21} are factors representing the physical conditions inherent in these populations. When r_1 , r_2 , a_{12} and a_{21} are positive, the solutions of the said model form closed orbits in the $\{x_1, x_2\}$ phase space. However, this model is unrealistic as it assumes that there is no limit to the prey the predator can consume, among other things. This is why Perez et. al. [20] showed a modification on Eq. (4.31) expressed as

$$\begin{cases} \dot{x}_1 = x_1 (+r_1 - a_{11}x_1 - a_{12}x_2) \\ \dot{x}_2 = x_2 (-r_2 + a_{21}x_1 - a_{22}x_2) \end{cases} \quad (4.32)$$

where $a_{11}x_1$ and $a_{22}x_2$ are terms imposing this limitation. Here, we see that DM and non-dynamic DE actually behaves like prey and predator in a simplified ecosystem as evident in the similar expressions between the modified Lotka-Volterra model and our dynamical system in Eq. (4.30).

4.2 Stability analysis of the system

We now set $\Omega'_{dm} = 0$ and $\Omega'_{de} = 0$. Solving these differential equations, we obtain our fixed points as shown in Table 4.1.

Table 4.1: Fixed points of system (4.30) and their corresponding eigenvalues and stability

| # | Ω_{dm}^* | Ω_{de}^* | Eigenvalues | Stability |
|---|--|------------------------|---|---|
| A | 0 | 0 | $-1, -1 - 3w_{\text{de}}$ | Saddle $\forall \epsilon, w_{\text{de}}$ |
| B | 1 | 0 | $1, -3w_{\text{de}} - \epsilon$ | Saddle for $\epsilon < -3w_{\text{de}}$ |
| C | 0 | 1 | $1 + 3w_{\text{de}}, 3w_{\text{de}} + \epsilon$ | Stable node for $\epsilon > -3w_{\text{de}}$ |
| D | $-\frac{1 + 3w_{\text{de}}}{\epsilon}$ | $\frac{1}{\epsilon}$ | $\pm \sqrt{\frac{(1 + 3w_{\text{de}})(3w_{\text{de}} + \epsilon)}{\epsilon}}$ | Saddle for $\epsilon < -3w_{\text{de}}$ Unstable node for $\epsilon > -3w_{\text{de}}$ Center for $\epsilon < -3w_{\text{de}}$ Saddle for $\epsilon > -3w_{\text{de}}$ |

Table 4.1 also shows the stability of these points as reflected by their corresponding eigenvalues which are calculated from the system's 2×2 Jacobian matrix in Eq.(4.33).

$$J(\Omega_{\text{dm}}^*, \Omega_{\text{de}}^*) = \begin{pmatrix} -1 + 2\Omega_{\text{dm}}^* + \Omega_{\text{de}}^*(1 + 3w_{\text{de}} + \epsilon) & \Omega_{\text{dm}}^*(1 + 3w_{\text{de}} + \epsilon) \\ \Omega_{\text{de}}^*(1 - \epsilon) & -1 - 3w_{\text{de}} + 2(1 + 3w_{\text{de}})\Omega_{\text{de}}^* + \Omega_{\text{dm}}^*(1 - \epsilon) \end{pmatrix} \quad (4.33)$$

4.3 Behavior of the system; phase plots

For a more complete qualitative evaluation of this cosmological model in which DM and non-dynamic DE are coupled by the given interaction term earlier, it would be useful to look into the system's phase plots shown in Figure 4.1. Recall Eq. (3.15) which shows that the curvature can be obtained from the abundance of other components in the universe. Note that the region below the solid black line ($\Omega_{\text{dm}} + \Omega_{\text{de}} = 1$) refers to values of $\Omega_{\text{dm}} + \Omega_{\text{de}} < 1$ which signifies a spatially-open (negatively curved) universe. On the other hand, the region above signifies a spatially-closed (positively curved) universe as it refers to values of $\Omega_{\text{dm}} + \Omega_{\text{de}} > 1$.

Figure 4.1a represents the case when $\epsilon > -3w_{\text{de}}$ where we see that a universe dominated by DM can evolve to a DE-dominated one, regardless of its curvature as evident in the nature of the blue and red trajectories. We also see other scenarios represented by the orange, magenta, and green trajectories for a spatially-closed universe. The orange curve indicates a scenario of initially decreasing DE and DM followed by an increase in DE until the universe becomes DE-dominated. On the other hand, a continuous decrease in DE and increase in DM are evident with the

curve colored in magenta. Finally, the green trajectory shows a DM-dominated universe evolving with an increase in both DM and DE.

On the other hand, when $\epsilon < -3w_{de}$ as represented in Figure 4.1b, a spatially-open (negatively curved) universe will exhibit periodic behavior between DM and DE where the former increases while the latter decreases and vice versa as shown by the blue trajectory. In contrast, the components of a spatially-closed (positively curved) universe evolves towards a continuously decreasing DE but increasing DM as shown by the red trajectory.

As we have mentioned in Chapter 2, one aspect of a dynamical system is its lack of time information. To supplement our analysis with this information, we consider the temporal evolution of Ω_{dm} and Ω_{de} for the blue trajectory when $\epsilon = 4$ which we present in Figure (4.2). In the said figure, we see periodic behavior in the evolution of these parameters which is expected from the cyclic curves the trajectory represents. Upon closer inspection, these oscillations have a period of about 9 e -foldings.

As we can see from our discussion, we do not need to solve for exact solutions of system (4.30) to obtain information about the evolution of its components. This becomes graphically available to us through phase plots. Such is the usefulness of dynamical systems. We will take advantage of this in analyzing the highly complicated cosmological model in the next chapter.

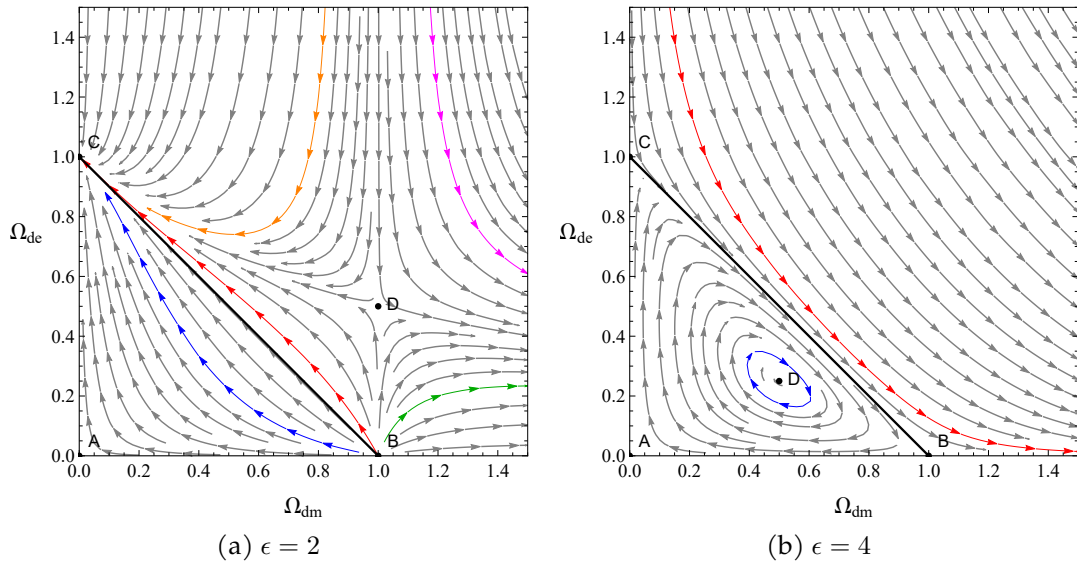


Figure 4.1: Phase plots of system (4.30) with $w_{de} = -1$ for different values of ϵ . (Note that other values of $w_{dm} < -1/3$ will not give any additional information. Thus, only cases of different ϵ were shown.) The solid black line pertains to $\Omega_{dm} + \Omega_{de} = 1$.

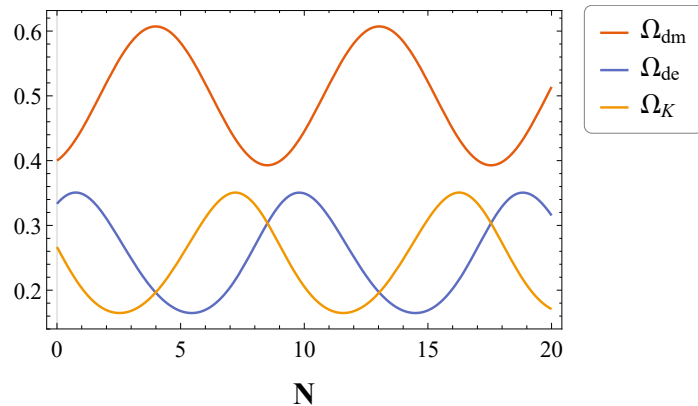


Figure 4.2: Evolution of cosmological parameters Ω_{dm} , Ω_{de} , Ω_K with respect to N for the blue trajectory in Figure 4.1b

Chapter 5

Coupling with dark matter and dynamic dark energy

So far, we have considered a non-dynamic dark energy in our discussion which is characterized by a constant EoS parameter. In this chapter, we finally construct a cosmological model in which dark matter interacts with dynamic dark energy that is now characterized by a time-varying EoS parameter. To do this, we need a field theory to mathematically depict how this dynamic DE changes according to our parameters. For the simplification of our calculations, we choose a time evolving scalar field $\phi = \phi(t)$ that is co-moving with the background (*i.e.* the scalar field is independent of the spatial components) to replace the non-dynamic dark energy in the model studied in the previous chapter as we will see in our discussion.

5.1 The dynamical system of x , y , and s

The Friedmann equations that characterize this cosmological scenario are similar to that of the model tackled in the previous chapter. However, we clarify that the scalar field does not automatically behave like dark energy as its EoS parameter must be less than $-1/3$ as mentioned in Chapter 3. Thus, to avoid confusion, we instead denote the variables pertaining to dark energy as those of the scalar field. We now write Eq. (4.1) as

$$\left(\frac{\dot{a}}{a}\right)^2 = \frac{\kappa^2}{3} (\rho_\phi + \rho_{\text{dm}}) - \frac{K}{a^2} \quad (5.1)$$

and Eq. (4.2) as

$$\frac{\ddot{a}}{a} = -\frac{\kappa^2}{6} ((\rho_\phi + \rho_{\text{dm}}) + 3(P_\phi + P_{\text{dm}})) \quad (5.2)$$

where the energy density and pressure of this field are calculated from the stress-energy tensor and are expressed as [31]

$$\rho_\phi = \frac{1}{2}\dot{\phi}^2 + V(\phi) \quad (5.3)$$

$$P_\phi = \frac{1}{2}\dot{\phi}^2 - V(\phi) \quad (5.4)$$

We define new variables x , y , and s where

$$x^2 = \frac{\kappa^2 \dot{\phi}^2}{6H^2}, \quad y^2 = \frac{\kappa^2 V(\phi)}{3H^2}, \quad s^2 = \frac{\kappa^2 \rho_{\text{dm}}}{3H^2} \quad (5.5)$$

not only because it is the usual convention, but also because it allows us to track the relative abundances of the scalar field's kinetic and potential energy which are pertained by x and y respectively. From this, it is expected that these variables has some relation with density parameters of the scalar field and dark matter. These expressions are shown in Eqs. (5.6) and (5.7).

$$\Omega_\phi = \frac{\kappa^2 \rho_\phi}{3H^2} = \frac{\kappa^2}{3H^2} \left[\frac{1}{2}\dot{\phi}^2 + V(\phi) \right] = \frac{\kappa^2 \dot{\phi}^2}{6H^2} + \frac{\kappa^2 V(\phi)}{3H^2} = x^2 + y^2 \quad (5.6)$$

$$\Omega_{\text{dm}} = s^2 \quad (5.7)$$

With these variables, along with the expressions of ρ_ϕ and P_ϕ in Eq. (5.3) and Eq. (5.4), we can arrange Eq. (5.1) into

$$1 = x^2 + y^2 + s^2 + \Omega_K \quad (5.8)$$

which shall impose a constraint in the degrees of freedom of this model in the same manner as Eq. (4.3). There is also the equation of parameter of the scalar field w_ϕ which is expressed as

$$w_\phi = \frac{P_\phi}{\rho_\phi} = \frac{\frac{1}{2}\dot{\phi}^2 - V(\phi)}{\frac{1}{2}\dot{\phi}^2 + V(\phi)} = \frac{\frac{3H^2 x^2}{\kappa^2} - \frac{3H^2 y^2}{\kappa^2}}{\frac{3H^2 x^2}{\kappa^2} + \frac{3H^2 y^2}{\kappa^2}} = \cancel{\frac{3H^2}{\kappa^2}} \frac{x^2 - y^2}{x^2 + y^2} = \frac{x^2 - y^2}{x^2 + y^2} \quad (5.9)$$

Now, note that the total EoS parameter w_{tot} must be less than $-1/3$ for the model to accommodate accelerated expansion. We can see this by tweaking Eq. (3.6) into an equation written for a combination of energy densities. Using (5.9), the total EoS parameter in terms of the newly defined variables is

$$w_{\text{tot}} = \frac{P_{\text{tot}}}{\rho_{\text{tot}}} = \frac{P_\phi + P_{\text{dm}}^0}{\rho_\phi + \rho_{\text{dm}}} = \frac{\frac{3H^2 x^2}{\kappa^2} - \frac{3H^2 y^2}{\kappa^2}}{\frac{3H^2 x^2}{\kappa^2} + \frac{3H^2 y^2}{\kappa^2} + \frac{3H^2 s^2}{\kappa^2}} = \frac{x^2 - y^2}{x^2 + y^2 + s^2} \quad (5.10)$$

Thus, the condition for accelerated expansion must be

$$\frac{x^2 - y^2}{x^2 + y^2 + s^2} < -\frac{1}{3} \quad (5.11)$$

Since Eq. (5.10) can only be negative if $x^2 < y^2$ (*i.e.* $\dot{\phi}^2 < V(\phi)$), it follows from the form of Eq. (5.9) that w_ϕ must be negative as well. We want the scalar field to drive this acceleration in the expansion even with the absence of dark matter so, from Eq. (5.11), the field must satisfy $w_\phi < -1/3$ for it to be considered as a dynamic dark energy component in the model.

As for the interaction term in this model, we would still be using $Q = \frac{\kappa^2}{3H} \epsilon \rho_\phi \rho_{\text{dm}}$. Since there have been a change of variables, it would be useful to express Q in terms of these variables. First, we consider

$$\begin{aligned} \rho_\phi \rho_{\text{dm}} &= \left[\frac{1}{2} \dot{\phi}^2 + V(\phi) \right] \rho_{\text{dm}} \\ &= \left[\frac{1}{2} \cancel{\frac{H^2}{\kappa^2}} x^2 + \frac{3H^2}{\kappa^2} y^2 \right] \frac{3H^2}{\kappa^2} s^2 \\ \rho_\phi \rho_{\text{dm}} &= [x^2 + y^2] \frac{9H^4}{\kappa^4} s^2 \end{aligned} \quad (5.12)$$

after substituting in Eq. (5.3) and applying Eq. (5.5). Then, by using this relation, we have

$$\begin{aligned} Q &= \frac{\kappa^2}{3H} \epsilon \rho_\phi \rho_{\text{dm}} \\ &= \frac{\kappa^2}{3H} \epsilon [x^2 + y^2] \frac{9H^4}{\kappa^4} s^2 \\ Q &= \frac{3H^3}{\kappa^2} \epsilon [x^2 + y^2] s^2 \end{aligned} \quad (5.13)$$

Also, with the similarity of the Friedmann equations, we note that the deceleration parameter would be in a similar form as that of Eq. (4.10). Applying the change of variables, we get

$$\begin{aligned} q &= \frac{1}{2} [(1 + 3w_\phi) \Omega_\phi + \Omega_{\text{dm}}] \\ &= \frac{1}{2} \left[\left(1 + 3 \frac{x^2 - y^2}{x^2 + y^2} \right) (x^2 + y^2) + s^2 \right] \\ &= \frac{1}{2} [(x^2 + y^2 + 3x^2 - 3y^2) + s^2] \\ &= \frac{1}{2} [(4x^2 - 2y^2) + s^2] \\ q &= 2x^2 - y^2 + \frac{1}{2}s^2 \end{aligned} \quad (5.14)$$

In this model, the energy conservation equations are also similar to those in Eqs. (4.13) and (4.14). However, with the time-evolving scalar field, Eq. (4.13) must be written as

$$\dot{\rho}_\phi + 3H(\rho_\phi + P_\phi) = -Q \quad (5.15)$$

which we can express as

$$\frac{d}{dt} \left(\frac{1}{2}\dot{\phi}^2 + V(\phi) \right) + 3H \left(\frac{1}{2}\dot{\phi}^2 + V(\phi) + \frac{1}{2}\dot{\phi}^2 - V(\phi) \right) = -Q \quad (5.16)$$

Note that

$$\frac{dV(\phi)}{dt} = \frac{dV(\phi)}{d\phi} \frac{d\phi}{dt} = \frac{dV(\phi)}{d\phi} \dot{\phi} \quad (5.17)$$

and that

$$\frac{d(\dot{\phi}^2)}{dt} = \frac{d(\dot{\phi}^2)}{d\dot{\phi}} \frac{d\dot{\phi}}{dt} = 2\dot{\phi}\ddot{\phi} \quad (5.18)$$

Thus, Eq. (5.16) becomes

$$\frac{1}{2}2\dot{\phi}\ddot{\phi} + \frac{dV(\phi)}{d\phi} \dot{\phi} + 3H\dot{\phi}^2 = -Q \quad (5.19)$$

Dividing the whole equation by $\dot{\phi}$

$$\ddot{\phi} + \frac{dV(\phi)}{d\phi} + 3H\dot{\phi} = -\frac{Q}{\dot{\phi}} \quad (5.20)$$

Therefore, we get

$$\ddot{\phi} = -\frac{dV(\phi)}{d\phi} - 3H\dot{\phi} - \frac{Q}{\dot{\phi}} \quad (5.21)$$

Now, for our dynamical system, we consider the prime derivatives of the curvature parameter and the defined variables in Eq. (5.5) through their dot derivatives. Since there has been no change with the curvature term the prime derivative of Ω_K will still be that in Eq. (4.23) which we will reiterate as follows:

$$\Omega'_K = 2q\Omega_K \quad (5.22)$$

However, in this model, q is now given by Eq. (5.14). As for the case of x' , we start

with

$$\begin{aligned}
\dot{x} &= \frac{dx}{dt} \\
&= \frac{d}{dt} \left(\frac{\kappa \dot{\phi}}{\sqrt{6}H} \right) \\
&= \frac{\kappa}{\sqrt{6}} \frac{d}{dt} \left(\frac{\dot{\phi}}{H} \right) \\
&= \frac{\kappa}{\sqrt{6}} \left(\frac{H\ddot{\phi} - \dot{\phi}\dot{H}}{H^2} \right) \\
\dot{x} &= \frac{\kappa}{\sqrt{6}} \left(\frac{\ddot{\phi}}{H} - \frac{\dot{H}}{H^2} \dot{\phi} \right)
\end{aligned} \tag{5.23}$$

Substituting in Eq. (5.21) and Eq. (3.11), \dot{x} becomes

$$\dot{x} = \frac{\kappa}{\sqrt{6}} \left[\frac{1}{H} \left(-\frac{dV(\phi)}{d\phi} - 3H\dot{\phi} - \frac{Q}{\dot{\phi}} \right) + (1+q)\dot{\phi} \right] \tag{5.24}$$

We let the potential to be $V(\phi) = V_0 e^{-\kappa\lambda\phi}$ where λ is a non-negative constant since it is a potential that allows us to no longer worry about ϕ as its derivative can be expressed as some constant multiplied with $V(\phi)$ itself. This is also a potential that drives inflation which is a period of accelerated expansion in our Universe so it is a good fit for modelling our dynamic dark energy. From this potential, we know that

$$\frac{dV(\phi)}{d\phi} = \frac{d}{d\phi} (V_0 e^{-\kappa\lambda\phi}) = -\kappa\lambda V_0 e^{-\kappa\lambda\phi} = -\kappa\lambda V(\phi) \tag{5.25}$$

Substituting Eqs. (5.25) into Eq. (5.24), we obtain

$$\begin{aligned}
\dot{x} &= \frac{\kappa}{\sqrt{6}} \left[\frac{1}{H} \left(\kappa\lambda V(\phi) - 3H\dot{\phi} - \frac{Q}{\dot{\phi}} \right) + (1+q)\dot{\phi} \right] \\
&= \frac{\kappa}{\sqrt{6}} \left[\frac{\kappa\lambda V(\phi)}{H} - \frac{3H\dot{\phi}}{H} - \frac{Q}{H\dot{\phi}} + (1+q)\dot{\phi} \right]
\end{aligned} \tag{5.26}$$

Plugging in Eq. (5.5),

$$\begin{aligned}
\dot{x} &= \frac{\kappa}{\sqrt{6}} \left[\frac{\kappa \lambda 3H^2}{H} y^2 - 3 \frac{\sqrt{6}H}{\kappa} x - \frac{\kappa}{\sqrt{6}H} \frac{1}{x} \frac{Q}{H} + (1+q) \frac{\sqrt{6}H}{\kappa} x \right] \\
&= \frac{\kappa}{\sqrt{6}} \frac{\kappa \lambda 3H^2}{H} \frac{y^2}{\kappa^2} - 3 \frac{\kappa}{\sqrt{6}} \frac{\sqrt{6}H}{\kappa} x - \frac{\kappa}{\sqrt{6}} \frac{\kappa}{\sqrt{6}H} \frac{1}{x} \frac{Q}{H} + (1+q) \frac{\kappa}{\sqrt{6}} \frac{\sqrt{6}H}{\kappa} x \\
&= \frac{3}{\sqrt{6}} \lambda H y^2 - 3 H x - \frac{\kappa^2}{6} \frac{1}{x} \frac{Q}{H^2} + (1+q) H x \\
&= \sqrt{\frac{3 \cdot 3}{2 \cdot 3}} \lambda H y^2 - 3 H x + (1+q) H x - \frac{\kappa^2}{6} \frac{1}{x} \frac{Q}{H^2} \\
\dot{x} &= H \left[\sqrt{\frac{3}{2}} \lambda y^2 - 3x + (1+q)x - \frac{\kappa^2}{6} \frac{1}{x} \frac{Q}{H^3} \right]
\end{aligned} \tag{5.27}$$

Recall the relation of an arbitrary quantity's dot derivative with its prime derivative in Eq. (3.17). From this, we can get x' by

$$x' = \frac{\dot{x}}{H} = \sqrt{\frac{3}{2}} \lambda y^2 - 3x + (1+q)x - \frac{\kappa^2}{6H^3} \frac{1}{x} Q \tag{5.28}$$

Substituting the interaction term in Eq. (5.28),

$$\begin{aligned}
x' &= \sqrt{\frac{3}{2}} \lambda y^2 - 3x + x(1+q) - \cancel{\frac{\kappa^2}{6H^3}} \frac{1}{x} \frac{3H^3}{\cancel{\kappa^2}} \epsilon (x^2 + y^2) s^2 \\
&= \sqrt{\frac{3}{2}} \lambda y^2 - 3x + x(1+q) - \frac{1}{2x} \epsilon (x^2 + y^2) s^2
\end{aligned} \tag{5.29}$$

On the other hand, for the case of y' , we first set up \dot{y} by

$$\begin{aligned}
\dot{y} &= \frac{dy}{dt} \\
&= \frac{d}{dt} \left(\frac{\kappa \sqrt{V(\phi)}}{\sqrt{3}H} \right) \\
&= \frac{\kappa}{\sqrt{3}} \frac{d}{dt} \left(\frac{\sqrt{V(\phi)}}{H} \right) \\
\dot{y} &= \frac{\kappa}{\sqrt{3}} \frac{1}{H^2} \left(H \cdot \frac{d}{dt} \left(\frac{\sqrt{V(\phi)}}{H} \right) - \sqrt{V(\phi)} \cdot \dot{H} \right)
\end{aligned} \tag{5.30}$$

Then, note that

$$\frac{d}{dt} \left(\frac{\sqrt{V(\phi)}}{H} \right) = \frac{d}{dV(\phi)} \frac{dV(\phi)}{d\phi} \frac{d\phi}{dt} = \frac{1}{2\sqrt{V(\phi)}} \frac{dV(\phi)}{d\phi} \dot{\phi} \tag{5.31}$$

For the given potential, its derivative with respect to ϕ is given by Eq. (5.25). Thus, \dot{y} can be expressed as

$$\begin{aligned}
\dot{y} &= \frac{\kappa}{\sqrt{3}} \frac{1}{H^2} \left(H \cdot \frac{1}{2\sqrt{V(\phi)}} \frac{dV(\phi)}{d\phi} \dot{\phi} - \sqrt{V(\phi)} \cdot \dot{H} \right) \\
&= \frac{\kappa}{\sqrt{3}} \frac{1}{H^2} \left[H \cdot \frac{1}{2\sqrt{V(\phi)}} (-\kappa\lambda V(\phi)) \dot{\phi} - \sqrt{V(\phi)} \cdot \dot{H} \right] \\
&= \frac{\kappa}{\sqrt{3}} \left[-\frac{\kappa\lambda}{2H} \sqrt{V(\phi)} \dot{\phi} - \sqrt{V(\phi)} \frac{\dot{H}}{H^2} \right] \\
&= -\frac{\kappa\lambda}{2H} \frac{\sqrt{3}H}{\sqrt{3}} y \frac{\sqrt{6}H}{\kappa} x + \frac{\kappa}{\sqrt{3}} \frac{\sqrt{3}H}{\kappa} y(1+q) \\
&= -\frac{\sqrt{6}}{2} \lambda H y x + H y(1+q) \\
\dot{y} &= H \left[-\sqrt{\frac{3 \cdot 2}{2 \cdot 2}} \lambda y x + y(1+q) \right]
\end{aligned} \tag{5.32}$$

by plugging in the defined variables and substituting \dot{H}/H^2 with the use of Eq. (3.11). Thus, in the same manner as that of x' , y' is given by

$$y' = \frac{\dot{y}}{H} = -\sqrt{\frac{3}{2}} \lambda y x + y(1+q) \tag{5.33}$$

Finally, for the case of s' , we begin with

$$\begin{aligned}
\dot{s} &= \frac{ds}{dt} \\
&= \frac{d}{dt} \left(\frac{\kappa \sqrt{\rho_{dm}}}{\sqrt{3}H} \right) \\
&= \frac{\kappa}{\sqrt{3}} \frac{d}{dt} \left(\frac{\sqrt{\rho_d}}{H} \right) \\
\dot{s} &= \frac{\kappa}{\sqrt{3}} \frac{1}{H^2} \left(H \cdot \frac{d(\sqrt{\rho_d})}{dt} - \sqrt{\rho_{dm}} \cdot \dot{H} \right)
\end{aligned} \tag{5.34}$$

Note that

$$\frac{d(\sqrt{\rho_d})}{dt} = \frac{d(\sqrt{\rho_d})}{d\rho_d} \frac{d\rho_d}{dt} = \frac{\dot{\rho}_d}{2\sqrt{\rho_d}} \tag{5.35}$$

Note that $\dot{\rho}_{dm}$ can be taken from its energy conservation equation in Eq. (4.14). Thus,

$$\frac{d(\sqrt{\rho_{dm}})}{dt} = \frac{Q - 3H\rho_{dm}}{2\sqrt{\rho_{dm}}} \tag{5.36}$$

Substituting this back to \dot{s} ,

$$\begin{aligned}
\dot{s} &= \frac{\kappa}{\sqrt{3}} \left(\frac{1}{H} \cdot \frac{Q - 3H\rho_{\text{dm}}}{2\sqrt{\rho_{\text{dm}}}} - \sqrt{\rho_{\text{dm}}} \cdot \frac{\dot{H}}{H^2} \right) \\
&= \frac{\kappa}{\sqrt{3}} \left(\frac{Q}{2H\sqrt{\rho_{\text{dm}}}} - \frac{3H\rho_{\text{dm}}}{2H\sqrt{\rho_{\text{dm}}}} - \sqrt{\rho_{\text{dm}}} \cdot \frac{\dot{H}}{H^2} \right) \\
&= \frac{\kappa}{\sqrt{3}} \cdot \frac{Q}{2H\sqrt{\rho_{\text{dm}}}} - \frac{\kappa}{\sqrt{3}} \cdot \frac{3}{2}\sqrt{\rho_{\text{dm}}} - \frac{\kappa}{\sqrt{3}} \cdot \sqrt{\rho_{\text{dm}}} \cdot \frac{\dot{H}}{H^2} \\
&= \frac{\kappa}{\sqrt{3}} \frac{Q}{2H\sqrt{3}Hs} - \frac{\kappa}{\sqrt{3}} \frac{3}{2} \frac{\cancel{\sqrt{3}}H}{\cancel{\kappa}} s + \frac{\kappa}{\sqrt{3}} \frac{\cancel{\sqrt{3}}H}{\cancel{\kappa}} s(1+q) \\
&= \frac{\kappa^2}{6H^2s} Q - \frac{3}{2} Hs + Hs(1+q) \\
\dot{s} &= Hs \left[\frac{\kappa^2}{6H^3s^2} Q \cancel{\frac{3}{2}}^{-\frac{1}{2}} + 1 + q \right]
\end{aligned} \tag{5.37}$$

after substituting s from Eq. (5.5) and Eq. (3.11). Thus, s' is given by

$$s' = \frac{\dot{s}}{H} = s \left[\frac{\kappa^2}{6H^3s^2} Q - \frac{1}{2} + q \right] \tag{5.38}$$

Plugging in Q from Eq. (5.13),

$$s' = s \left[\frac{\kappa^2}{6H^3} \cancel{\frac{1}{2}} \frac{1}{\cancel{\kappa^2}} \frac{3H^3}{\cancel{\kappa^2}} \epsilon (x^2 + y^2) \cancel{\frac{3}{2}} - \frac{1}{2} + q \right] = s \left[\frac{1}{2} \epsilon (x^2 + y^2) - \frac{1}{2} + q \right] \tag{5.39}$$

Now, this model where dark matter and a scalar field interact with each other is fully characterized by the system made up of Eqs. (5.22), (5.29), (5.33), and (5.39), along with Eq. (3.19). Due to reasons mentioned before, however, we can opt not to include Eqs. (3.19) and (5.22) in our analysis. This leads to

$$\begin{cases} x' = \sqrt{\frac{3}{2}} \lambda y^2 - 3x + x(1+q) - \frac{1}{2x} \epsilon (x^2 + y^2) s^2 \\ y' = -\sqrt{\frac{3}{2}} \lambda yx + y(1+q) \\ s' = s \left[\frac{1}{2} \epsilon (x^2 + y^2) - \frac{1}{2} + q \right] \end{cases} \tag{5.40}$$

as our dynamical system with state variables x , y , and s where q is a function of these variables calculated in Eq. (5.14). Since we still kept the scale factor general

as we constructed this model, the behavior of system 5.40 should also hold for all expressions of $a(t)$ like the previous model.

Since the derivation of our system is quite complicated, it would be helpful to check if the expressions we derived are right. To do this, we again consider dark matter interactions with non-dynamic dark energy that is tackled in the last chapter. The scalar field case discussed in this chapter has an additional degree of freedom brought about by the splitting of its energy density ρ_ϕ into kinetic and potential energy terms as stated in Eq. (5.3). This, in turn, required the cosmological model to have another evolution equation that is given by Eq. (5.21). However, note that the dynamic systems of both cases come from the same Friedmann equations so we should be able to recover one from the other, in theory, given certain conditions. Thus, we can check if the system we obtained in the scalar field case is correct by applying a change of variables using Eq. (5.5) to the system of the non-dynamic energy case that is stated in Eq. (4.30), along with Eq. (5.21). We show this check in Appendix A.

5.2 Stability analysis of the system

In the same manner as the previous chapter, we obtain the fixed points of the system in Eq. (5.40). We again note that ϵ and λ are non-negative constants. There are actually 22 of these points but we consider only 14 of them as these are the relevant points in our analysis. These considered points are tabulated in Table 5.1. The placeholders α , β , and γ for the expressions of points G_\pm and H_\pm are defined as

$$\alpha = \frac{-6\lambda + 2\epsilon\lambda - 2\sqrt{36\epsilon - 12\epsilon^2 + 9\lambda^2 - 6\epsilon\lambda^2 + \epsilon^2\lambda^2}}{4\sqrt{6}\epsilon} \quad (5.41)$$

$$\beta = \sqrt{18 + 6\epsilon + \frac{9\lambda^2}{\epsilon} - \epsilon\lambda^2 + \lambda\sqrt{36\epsilon - 12\epsilon^2 + 9\lambda^2 - 6\epsilon\lambda^2 + \epsilon^2\lambda^2}} + \frac{3\lambda\sqrt{36\epsilon - 12\epsilon^2 + 9\lambda^2 - 6\epsilon\lambda^2 + \epsilon^2\lambda^2}}{\epsilon} \Bigg/ (2\sqrt{3\epsilon}) \quad (5.42)$$

$$\gamma = \frac{\sqrt{-6 + 2\epsilon + \lambda^2 - \frac{3\lambda^2}{\epsilon} - \frac{\lambda\sqrt{36\epsilon - 12\epsilon^2 + 9\lambda^2 - 6\epsilon\lambda^2 + \epsilon^2\lambda^2}}{\epsilon}}}{\sqrt{2\epsilon}} \quad (5.43)$$

Table 5.1: Existence of fixed points

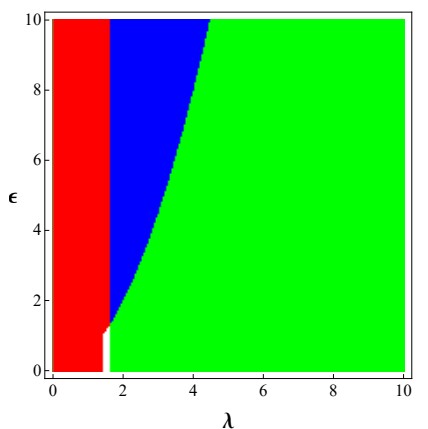
| # | x^* | y^* | s^* | Existence |
|---------------------|--|---|---|----------------------------------|
| A | -1 | 0 | 0 | $\forall \lambda, \epsilon$ |
| B | 1 | 0 | 0 | $\forall \lambda, \epsilon$ |
| C_{\pm} | $\frac{1}{\lambda} \sqrt{\frac{2}{3}}$ | $\pm \frac{2}{\sqrt{3}\lambda}$ | 0 | $\forall \lambda, \epsilon$ |
| $D_{\pm} [E_{\pm}]$ | $\frac{1}{\lambda} \sqrt{\frac{2}{3}}$ | $-[+] \sqrt{\frac{3 - \frac{2\epsilon}{\lambda^2}}{3\epsilon}}$ | $\pm \frac{1}{\lambda^2} \sqrt{\frac{2(-2\epsilon + \lambda^2)}{\epsilon}}$ | $\epsilon < \frac{\lambda^2}{2}$ |
| F_{\pm} | $\frac{\lambda}{\sqrt{6}}$ | $\pm \sqrt{\frac{6 - \lambda^2}{6}}$ | 0 | $\lambda < \sqrt{6}$ |
| $G_{\pm} [H_{\pm}]$ | α | $-[+] \beta$ | $\pm \gamma$ | See Figure 5.1b |

As for their corresponding eigenvalues and stability, we present these in Table 5.2. The eigenvalues of D_{\pm} , E_{\pm} , G_{\pm} , and H_{\pm} are roots of long and complicated expressions so we do not show them here. Since we cannot provide an analytic distinction on the stability of these points from the eigenvalues, we graphically present their stability in a $\{\lambda, \epsilon\}$ parameter space along with that of C_{\pm} in Figure 5.1. Also, the 3×3 Jacobian matrix from which the eigenvalues were calculated from is

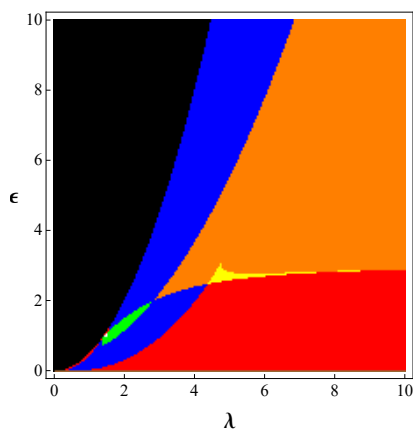
$$J(x^*, y^*) = \begin{pmatrix} -2 + 6x^{*2} - y^{*2} + \frac{1}{2}s^{*2} \left(1 + \left(-1 + \frac{y^2}{x^2} \right) \epsilon \right) \\ 4x^*y^* - \sqrt{\frac{3}{2}}y^*\lambda \\ s^*x^*(4 + \epsilon) \\ y^* \left(-2x^* - \frac{s^{*2}\epsilon}{x^*} + \sqrt{6}\lambda \right) \\ \frac{1}{2}(2 + s^{*2} + 4x^{*2} - 6y^{*2} - \sqrt{6}x^*\lambda) \\ s^*y^*(-2 + \epsilon) \\ s^* \left(x^* - x^*\epsilon - \frac{y^{*2}\epsilon}{x^*} \right) \\ s^*y^* \\ \frac{1}{2}(-1 + 3s^{*2} - 2y^{*2} + y^{*2}\epsilon + x^{*2}(4 + \epsilon)) \end{pmatrix} \quad (5.44)$$

Table 5.2: Stability of fixed points

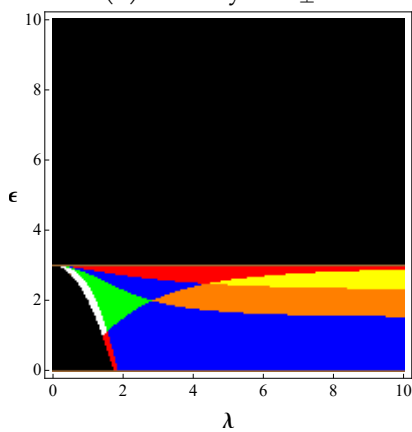
| # | Eigenvalues | Stability |
|--------------------|---|--|
| A | $4, \frac{1}{2}(3 + \epsilon), \frac{1}{2}(6 + \sqrt{6}\lambda)$ | Unstable node $\forall \lambda$ |
| B | $4, \frac{1}{2}(3 + \epsilon), \frac{1}{2}(6 - \sqrt{6}\lambda)$ | Unstable node for $\lambda < \sqrt{6}$ Saddle for $\lambda > \sqrt{6}$ |
| C_{\pm} | $\frac{2\epsilon - \lambda^2}{2\lambda^2}, -1 \pm \frac{\sqrt{8\lambda^2 - 3\lambda^4}}{\lambda^2}$ | See Figure 5.1a |
| D_{\pm}, E_{\pm} | - | See Figure 5.1b |
| F_{\pm} | $\frac{1}{2}(-6 + \lambda^2), -2 + \lambda^2,$ $\frac{1}{2}(-3 + \epsilon + \lambda^2)$ | Stable node for $\epsilon < 3 - \lambda^2$ where $\lambda < \sqrt{2}$ Saddle for $\lambda < \sqrt{6}$ except for stable node region |
| G_{\pm}, H_{\pm} | - | See Figure 5.1c |



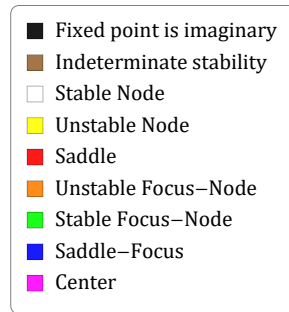
(a) Stability of C_{\pm}



(b) Stability of D_{\pm} and E_{\pm}



(c) Stability of G_{\pm} and H_{\pm}



(d) Legend

Figure 5.1: $\{\lambda, \epsilon\}$ parameter space indicating the stability of certain fixed points

5.3 Cosmological parameters of the fixed points

We did not explicitly discuss the cosmological parameters of the fixed points in the previous cosmological model since the state variables in that system are the cosmological parameters themselves. On the other hand, we need a bit more insight for this system to clearly see what these fixed points physically represent. Thus, we have tabulated the expressions for these parameters in Table 5.3.

Table 5.3: Cosmological parameters of fixed points where we let $\delta = \epsilon(-6 + \lambda^2)$ and $\Delta = \sqrt{(-3 + \epsilon)(-3\lambda^2 + \epsilon(-12 + \lambda^2))}$

| # | w_ϕ | w_{tot} | Ω_ϕ | Ω_{dm} | Ω_K |
|----------------|-------------------------------------|--|--|--|--|
| A, B | 1 | 1 | 1 | 0 | 0 |
| C_\pm | $-\frac{1}{3}$ | $-\frac{1}{3}$ | $\frac{2}{\lambda^2}$ | 0 | $1 - \frac{2}{\lambda^2}$ |
| D_\pm, E_\pm | $-1 + \frac{4\epsilon}{3\lambda^2}$ | $-\frac{1}{3}$ | $\frac{1}{\epsilon}$ | $\frac{2}{\epsilon} - \frac{4}{\lambda^2}$ | $1 - \frac{3}{\epsilon} - \frac{4}{\lambda^2}$ |
| F_\pm | $\frac{1}{3}(-3 + \lambda^2)$ | $\frac{1}{3}(-3 + \lambda^2)$ | 1 | 0 | 0 |
| G_\pm, H_\pm | $-\frac{\epsilon}{3}$ | $\frac{\delta + \lambda(-3\lambda + \Delta)}{6\epsilon}$ | $\frac{-\delta + \lambda(3\lambda - \Delta)}{2\epsilon^2}$ | $1 + \frac{\delta + \lambda(-3\lambda + \Delta)}{2\epsilon^2}$ | 0 |

- **Points A and B** pertain to scalar field-dominated universes with no curvature. Considering that $y = 0$ for these points, which means the absence of potential energy, this field is composed only of kinetic energy that has a stiff equation of state $P_\phi = \rho_\phi$ from the value of w_ϕ . Thus, that the scalar field behaves like stiff matter or a cold gas of baryons [8]. The expansion these universes is decelerating since $w_{\text{tot}} = 1$.
- **Points C_\pm** are scalar field-dominated universes whose abundance curvature depends on the value of λ . When $\lambda < [>]\sqrt{2}$, the curvature becomes positive [negative]. For $\lambda = \sqrt{2}$, this value of λ yields $\Omega_\phi = 1$ and $\Omega_K = 0$ like points A and B. However, this time, the scalar field has an EoS parameter $w_\phi = -1/3$. With w_{tot} having the same value, the expansion in such universes is neither accelerating or decelerating.
- **Points D_\pm and E_\pm** pertain to universes in which the abundances of its components are dependent on the value of ϵ and λ . Although Ω_{dm} can become negative when $\epsilon > \lambda^2/2$, we do not concern ourselves this because the fixed point itself becomes imaginary when $\epsilon > \lambda^2/2$. The scalar

field in this case can behave like dark energy when $\epsilon < \lambda^2/2$. However, the expansion such universes is still neither accelerating or decelerating since $w_{\text{tot}} = -1/3$, independent of ϵ and λ . This suggests that dynamic dark energy does not dominate in these universes.

- **Points F_{\pm}** are flat scalar field-dominated universes in which the scalar field can behave like dark energy when $\lambda < \sqrt{2}$ while accelerated expansion is achieved within the same range of values.
- **Points G_{\pm} and H_{\pm}** are flat universes in which the abundances of the scalar field and dark matter are dependent on the value of ϵ and λ . The scalar field acts like dark energy when $\epsilon > 1$. The other cosmological parameters (*i.e.* w_{tot} , Ω_ϕ , and Ω_{dm}) have complicated expressions so no further analysis can be made.

5.4 System behavior and phase plots

In our phase plots, there are certain regions of interest which are shaded for convenience. The yellow region pertains to $x^2 + y^2 + s^2 < 1$ or, equivalently, $\Omega_\phi + \Omega_{\text{dm}} < 1$ and forms a sphere in the 3D phase space. The region not included in this sphere pertains to $x^2 + y^2 + s^2 > 1$ or, equivalently, $\Omega_\phi + \Omega_{\text{dm}} > 1$. Recall that the curvature can be inferred from the values of the other components in the universe as shown in Eq. (3.15). These just mean that points in the yellow region represent universes that are negatively curved while those outside of this region are positively curved. The points at the boundary that separates these two regions of curvature are flat universes. On the other hand, the region where the scalar field acts like dark energy is shaded in cyan.

From the possible combinations of the fixed points' stabilities for a given λ and ϵ , there are a lot of qualitatively different phase spaces that we can look into. Moreover, we are dealing with a 3D phase space so there are a whole lot more trajectories than those in the 2D dynamical system that we had discussed in Chapter 4. Due to this, our analysis can become quite complicated and cannot be as extensive as in the previous model where we can point out all the qualitatively different trajectories in all possible phase plots of the system. Fortunately, the phase spaces of this system that we have studied so far at least have certain features that can simplify it.

One feature is that we can look at the positive and negative x regions independently except for some surfaces like the $s = 0$ plane as we will see later. Barring these exceptions, trajectories from one region do not cross over to the other region which we notice from a sample phase plot in Figure 5.2a. This is due to the fact that the phase space of system (5.40) has a discontinuity at the $x = 0$ plane which is physically a universe with a cosmological constant as its dark energy. We can attribute this discontinuity to the $1/x$ term in the differential of x (Eq. (5.29)).

Now, although this feature does simplify our analysis, it is also quite troublesome since the $x = 0$ plane becomes inaccessible which leads to information loss in that surface. One way to resolve this is apply a change of variables where $x = 0$ is no longer discontinuous. A natural variable change would be from x,y,s to x^2,y^2,s^2 . In other words, we would obtain a dynamical system that represents the evolution of x^2,y^2,s^2 instead of system (5.40). However, the fixed points of this system have complicated analytical expressions that we cannot apply the same analysis as we have done on system (5.40) with the time frame we have so we leave this as a possible future work.

Another simplifying feature is that the fixed points and trajectories in one quadrant of the positive x region, as well as those the negative x region, are reflected to the other quadrants. This can be seen in the similarities of the sample trajectories and position of the fixed points with respect to the four quadrants of Figures 5.2b and 5.2c. Thus, by reflection symmetry, we can just focus on one quadrant for each region when looking for qualitatively different trajectories and fixed points.

Moving on, recall that the goal of this thesis is to look into the late-time dynamics of this cosmological model with dark matter and dynamic dark energy. In relation to the possible end states of this model, we can generally classify our phase plots into three cases with respect to the number of stable fixed points. A phase space can either have none (case 1), one (case 2), or two (case 3) of these points. In Figure 5.3, we can see which values of λ and ϵ will result to one of these cases. We note that there are actually three stable points for $\lambda = 2$ and $\epsilon = 1.5$ but two of these points occupy the same position in the phase space so we consider them into the third case. Also, these stable points can technically be more than the said numbers when we look at the full phase space. However, we just considered those in one quadrant due to reflection symmetry which led to the said classification.

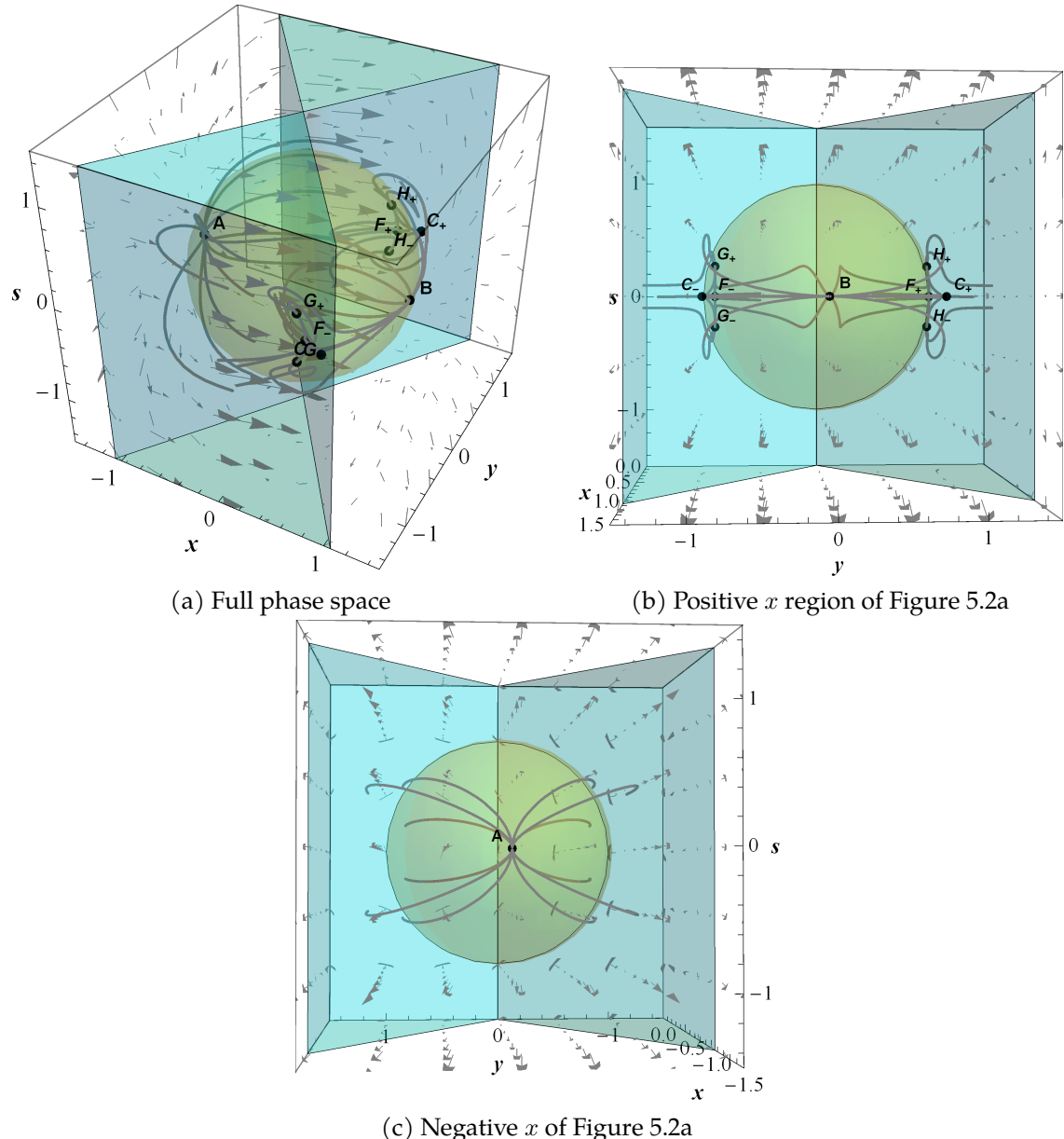


Figure 5.2: A phase plot of system (5.40) with $\lambda = 1.2$ and $\epsilon = 1.9$ with sample trajectories in gray

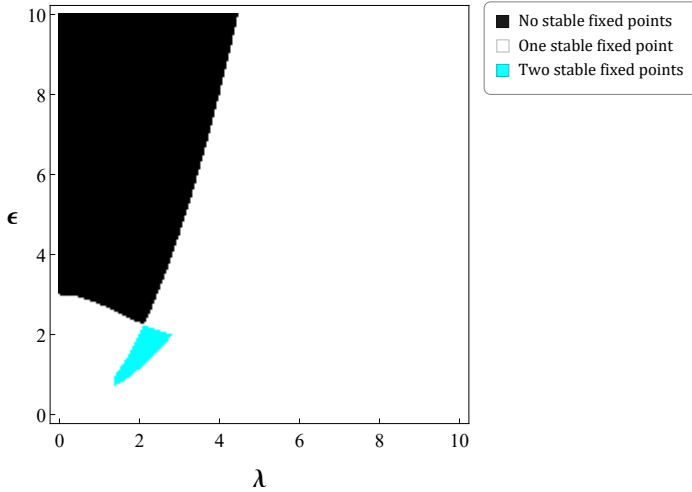


Figure 5.3: $\{\lambda, \epsilon\}$ parameter space indicating the classification of phase plots

Region of negative x : All cases

Let us first discuss these cases in the context of the negative x region. For case 1, we look at a phase plot when $\lambda = 1$ and $\epsilon = 4$ as shown in Figure 5.4a. Here, we can distinguish four distinct behaviour of trajectories represented in sandy brown, blue violet, steel blue, and forest green. The first two are spatially-open universes with decreasing kinetic energy of ϕ along with increasing potential energy and dark matter, though the sandy brown trajectory exhibits an immediate decrease in kinetic energy followed by a relatively more gradual one. This would be the opposite of the blue violet curve which starts out with a gradual decrease followed by a relatively more immediate one. The steel blue curve is a flat or spatially-closed universe that imitate the behavior of the blue violet trajectory. On the other hand, the forest green curve is a spatially-closed universe that shows an increase in kinetic energy before decreasing, again with increasing potential energy and dark matter. When we look at the trajectories in the phase plots of other cases (Figures 5.4b and 5.4c), we see that their behavior generally mimics those of case 1. Therefore, we observe a general behavior of trajectories moving away from point A towards the $x = 0$ plane in this region no matter which case the phase plot belongs to.

Region of positive x : Case 1 (No stable fixed points)

In the context of the positive x region, let us start at the first case in which there are no stable fixed points in the phase space. Looking at the phase plot when $\lambda = 1$ and $\epsilon = 4$ as shown in Figure 5.5a, we find at least ten qualitatively different trajectories

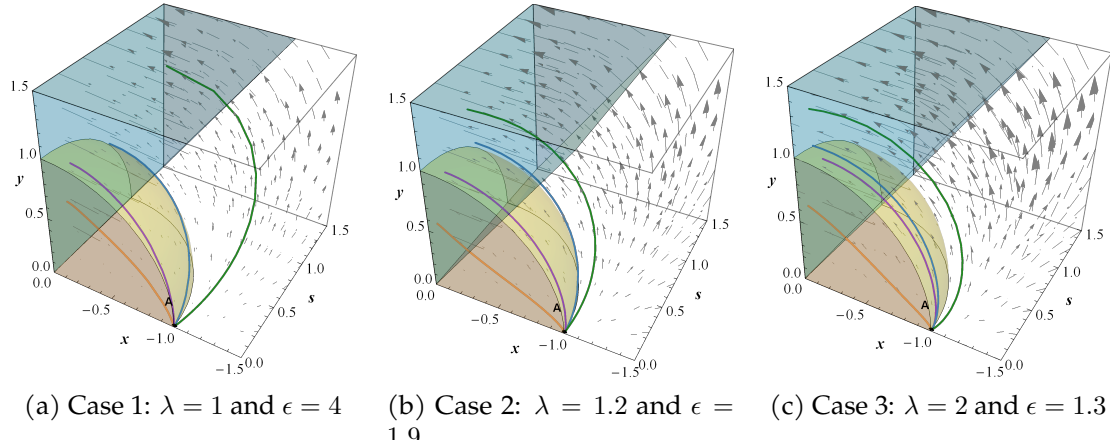


Figure 5.4: Quadrants of the considered phase plots in the negative x region with sandy brown, blue violet, steel blue, and forest green trajectories to represent the different qualitative trajectories in this region. Point A is an unstable node in all these cases

depicted in different colors. The yellow green, blue, and magenta curves initially move away from the $x = 0$ plane in which first two of these trajectories are positively curved while the latter is negatively curved. After being repelled by a saddle point, which in this case is C_+ , the blue trajectory generally increases in x before decreasing. The green trajectory, on the other hand, exhibits a more immediate decrease after being repelled. This behavior can also be seen in the magenta curve but the saddle point in question is now F_+ . As for the other trajectories, they initially move away from point B which is an unstable node. The yellow, purple, and cyan trajectories generally exhibit similar behavior in the latter stages of their evolution to that of blue, yellow green, and magenta respectively. The pink and red curves start out with a gradual decrease in x followed by a relatively more immediate one but the former is positively curved while the latter is negatively curved. The sea green trajectory initially follows the behavior of the red one until we see a decrease in s in the latter stages of its evolution. Finally, there is the orange red curve which starts out like the cyan curve but exhibits a relatively more abrupt decrease in x later on.

As for when $\lambda = 1.2$ and $\epsilon = 8$ as presented in Figure 5.5b, we find almost the same trajectories as that of the previous phase plot. However, we no longer see trajectories represented in purple and there is a new behavior of curves portrayed by the teal trajectory. This trajectory starts out moving away from the $x = 0$ plane and then repelled by the saddle point F_+ and the now saddle-focus point C_+ . On the

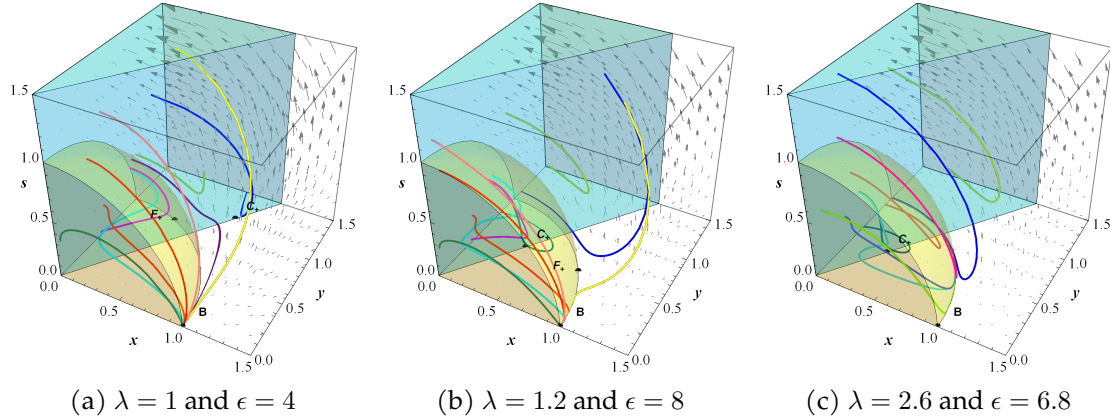


Figure 5.5: Quadrants of the considered phase plots in the positive x region for the first case. The qualitatively different curves are represented in purple, cyan, blue, red, yellow green, yellow, orange red, magenta, pink, sea green, teal, chartreuse, turquoise, deep pink, indian red, and royal blue.

other hand, the curves in the phase plot when $\lambda = 2.6$ and $\epsilon = 6.8$ no longer have trajectories that starts out by moving away from B which is now a saddle point so all the trajectories starts out moving away from the $x = 0$ plane. We still see the blue, yellow green, and teal trajectories as shown in Figure 5.5c. There are new trajectories but they generally exhibit similar behavior in the latter stages of their evolution as to those in the phase plots discussed earlier. For instance, the curves represented by the chartreuse, turquoise, deep pink, indian red, and royal blue trajectories are similar to those represented by sea green, cyan, pink, red, and the orange red trajectories.

There are definitely numerous trajectories for this case. We have seen at least sixteen qualitatively different curves from Figure 5.5. Nevertheless, we can see that all these curves eventually move towards the $x = 0$ plane.

Region of positive x : Case 2 (One stable fixed point)

From here on, note that we no longer represent trajectories that end up moving towards the $x = 0$ plane in colored curves because we already discussed most, if not all, of them in the first case. Furthermore, we already know their end states and we would have an easier time in reading the phase plots if we no longer represent them. Starting at the phase plot when $\lambda = 1.2$ and $\epsilon = 1.9$ as shown in Figure 5.6a, we find at least six qualitatively different trajectories which are represented by dark red, dark orange, dark green, dark blue, gold, and brown curves. We see that the initial stages of evolution for the dark green and brown trajectories are similar to that of

cyan and magenta. The difference is that they are now attracted towards the stable fixed point H_+ . These trajectories start out as negatively curved, evolving towards a flat universe later on. As for the other four, they start out as negatively curved and also evolve towards a flat universe. The red trajectory represent curves moving away from the unstable point B which are attracted to and then repelled from the saddle point C_+ before finally ending up at H_+ . The initial stages of evolution for the dark orange curve are similar to that of the dark red one but this trajectory is also attracted to and then repelled from another saddle point, F_+ , before moving towards H_+ . The dark blue and gold-colored curves are similar to the dark orange and dark red curves. However, instead of initially moving away from B , they initially move away from the $x = 0$ plane.

In the phase plane when $\lambda = 1.5$ and $\epsilon = 2$ as presented in Figure 5.6b, H_+ becomes a stable focus-node. We no longer see curves portryed by dark blue, gold, and dark orange trajectories. Instead, we find curves represented by the saddle brown and red violet trajectories. The former spirals toward H_+ while the latter do so after being repelled from C_+ . Our trajectories completely change when $\lambda = 5$ and $\epsilon = 4$ which are depicted in olive green, dark magenta, and navy blue. C_+ becomes the stable focus-node while points F_+ and H_+ vanishes. Furthermore, E_+ appear as an unstable focus-node. The olive trajectory in this plot represent curves moving away from E_+ towards C_+ . Both the dark magenta and navy blue curves start out moving away from the $x = 0$ plane towards the stable point. The difference is that the former exhibits a general increase in s or in dark matter before decreasing as it evolves towards C_+ . On the other hand, we do not see this in the latter trajectory. Finally, we have the dark slate blue trajectory which we see the phase plot when $\lambda = 2$ and $\epsilon = 1.3$ as shown in Figure 5.6d. As E_+ is now a saddle focus point, this curve starts out near the $x = 0$ plane and spirals toward the said point before being repelled to C_+ .

From these sample phase plots for this case, we see that most of the trajectories still behave like those of in the previous case. However, there is now a stable point where some of the trajectories are attracted to go. Therefore, there are two possible end states in this case which are those moving towards the $x = 0$ plane and those moving towards the stable point.

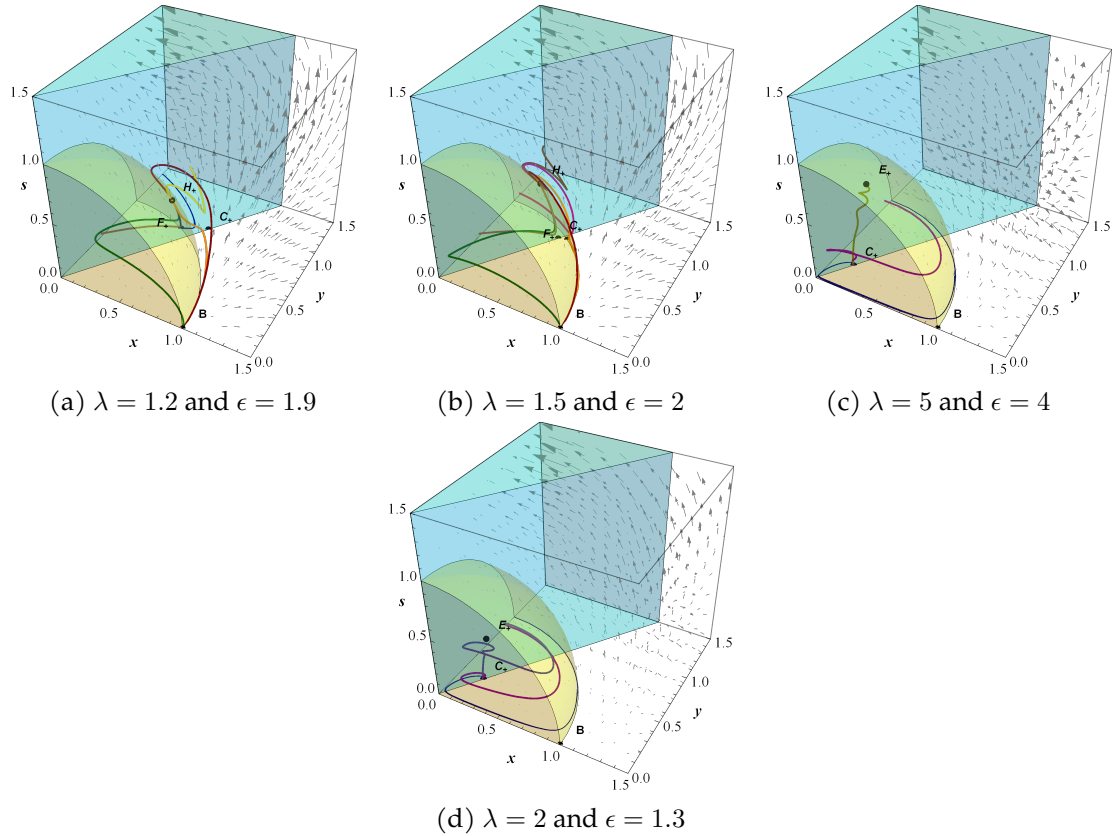


Figure 5.6: Quadrants of the considered phase plots in the positive x region for the second case. The qualitatively different curves are represented in dark red, dark orange, dark green, dark blue, gold, brown, saddle brown, red violet, dark magenta and navy blue.

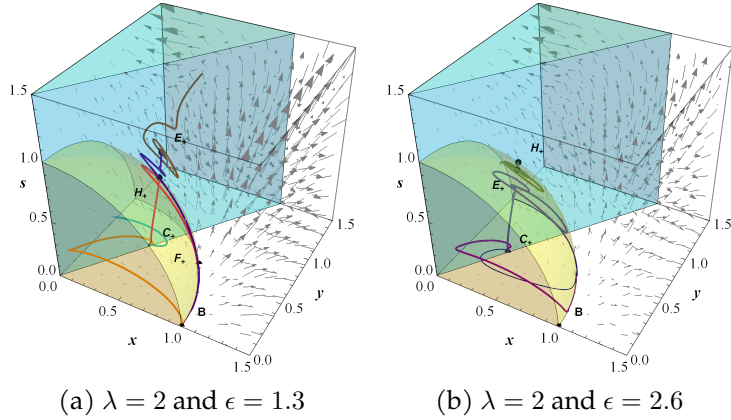


Figure 5.7: Quadrants of the considered phase plots in the positive x region for the third case. The qualitatively different curves are represented in saddle brown, indigo, crimson, orange, light sea green, dark magenta, navy blue, dark slate blue, and dark olive green.

Region of positive x : Case 3 (Two stable fixed points)

Finally for the third case, we find that there are similar curves from the second case like the saddle brown trajectory when $\lambda = 2$ and $\epsilon = 1.3$ as presented in Figure 5.7a. There are also the dark slate blue, dark magenta, and navy blue trajectories when $\lambda = 2$ and $\epsilon = 2.6$ as shown in Figure 5.7a. However, the saddle brown curve now spirals toward E_+ as it is the stable focus-node in its phase plot. Other curves in the said plot are represented by indigo, crimson, orange, and light sea green. The indigo trajectory is a positively curved trajectory that starts out near the unstable point B and then repelled by the saddle point F_+ and saddle focus H_+ before spiralling towards E_+ . The initial stages of evolution for the negatively curved crimson trajectory are similar to that of the indigo one but this trajectory is attracted towards the other stable focus-node C_+ . The orange curve also portray a negatively curved universe and initially evolves similar to the dark green and cyan trajectories in the previous cases. However, it is no longer repelled by a saddle point as it moves toward C_+ . On the other hand, the initial evolution of the light sea green trajectory is quite similar to the teal trajectory in the first case but its end state is now C_+ . As for Figure 5.7a, we see a negatively curved dark olive green trajectory spiralling towards the stable focus-node point of this plot which is H_+ .

From these sample phase plots for this case, we see that the addition of another stable point just increases the number of possible end states of the system into three with most of the trajectories still moving towards the $x = 0$.

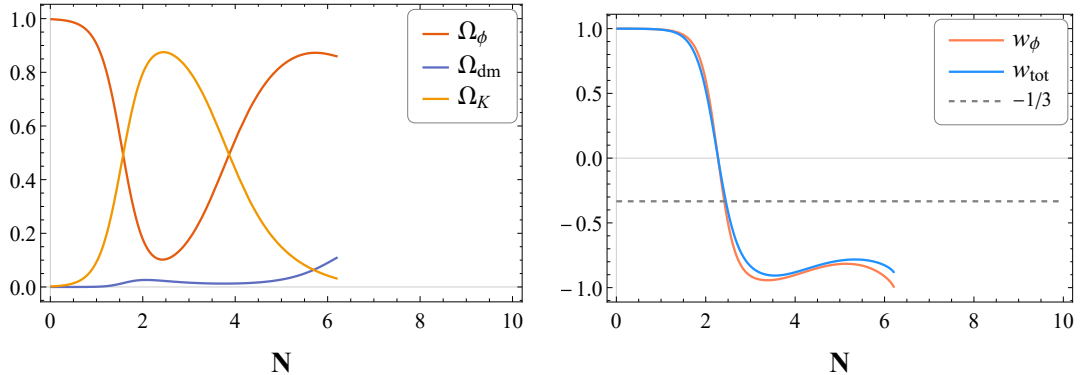


Figure 5.8: Evolution of cosmological parameters Ω_ϕ , Ω_{dm} , Ω_K , w_ϕ , and w_{tot} with respect to N for the cyan trajectory in Figure 5.5a

Temporal evolution of cosmological parameters for sample trajectories

In the same manner as in the previous chapter, we present here the evolution of cosmological parameters with respect to N of sample trajectories to supplement our phase plots with time information. In Figure 5.8, we show the said evolution for the cyan trajectory as an example for trajectories moving towards the $x = 0$ plane. We see that the curves get cut-off at some certain value of N . This is because integration of the solutions becomes inapplicable once they reach the discontinuity at $x = 0$. We also see that w_ϕ approaches -1 at the late stages of the cyan trajectory's evolution which shows that universes represented by trajectories moving towards the $x = 0$ plane end up with the cosmological constant as its dark energy component. On the other hand, Figure 5.9 is an example for trajectories moving towards a stable point and shows the temporal evolution of the saddle brown trajectory. Since this trajectory has a characteristic of spiraling towards the fixed point, we see oscillatory behavior in its temporal evolution which is most evident in w_ϕ and w_{tot} . We also see the curves flattening in about 15 to 20 e-foldings which indicate the arrival of the trajectory at the stable point. This shows that universes represented by trajectories ending up at stable points will reflect the cosmological parameters of these points (discussed in Section 5.3) after a certain period of time and will do so until the end of time.

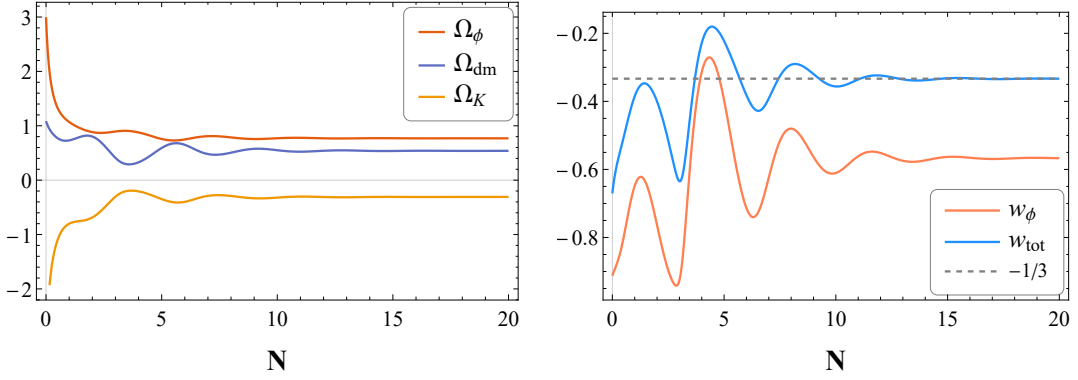


Figure 5.9: Evolution of cosmological parameters Ω_ϕ , Ω_{dm} , Ω_K , w_ϕ , and w_{tot} with respect to N for the saddle brown trajectory in Figure 5.7a

5.5 Analysis on the plane of $s = 0$

We have already mentioned before the plane $s = 0$ as an exception to our earlier analysis. This plane is special since it is an invariant manifold of system (5.40). This is, by no means, the only invariant manifold in the said system but we will limit our discussion of such a manifold to this plane not only because it can add to our analysis in the full phase space, but also of its possible underlying analogy to mechanics.

Now, this plane physically means a universe filled only with the kinetic and potential energies of the scalar field and the dynamics of such a universe is given by

$$\begin{cases} x' = \sqrt{\frac{3}{2}}\lambda y^2 - 3x + x(1+q) \\ y' = -\sqrt{\frac{3}{2}}\lambda yx + y(1+q) \end{cases} \quad (5.45)$$

where the deceleration parameter is now $q = 2x^2 - y^2$. This system is ϵ -independent due to the interaction term Q being non-existent for there is no dark matter to interact with the scalar field. We also want to note that $x = 0$ is no longer a discontinuity as the absence of dark matter removes the $1/x$ term in our system.

As we have done before, we can determine fixed points of this system which are shown in Table 5.4 and analyze their stability from eigenvalues as shown 5.5. The corresponding Jacobian matrix is given by

$$J(x^*, y^*) = \begin{pmatrix} -2 + 6x^{*2} - y^{*2} & -2x^*y^* + \sqrt{6}y^*\lambda \\ 4x^*y^* - \sqrt{\frac{3}{2}}y^*\lambda & 1 + 2x^{*2} - 3y^{*2} - \sqrt{\frac{3}{2}}x^*\lambda \end{pmatrix} \quad (5.46)$$

We note that the lower case letter labels are intentional to correlate the fixed points in this subspace to those in the full phase space with the exception of point i which has no corresponding fixed point.

Table 5.4: Existence of fixed points for system (5.45)

| # | x^* | y^* | Existence |
|---------|--|--------------------------------------|----------------------|
| a | -1 | 0 | $\forall \lambda$ |
| b | 1 | 0 | $\forall \lambda$ |
| c \pm | $\frac{1}{\lambda} \sqrt{\frac{2}{3}}$ | $\pm \frac{2}{\sqrt{3}\lambda}$ | $\forall \lambda$ |
| f \pm | $\frac{\lambda}{\sqrt{6}}$ | $\pm \sqrt{\frac{6 - \lambda^2}{6}}$ | $\lambda < \sqrt{6}$ |
| i | 0 | 0 | $\forall \lambda$ |

Table 5.5: Stability of fixed points

| # | Eigenvalues | Stability |
|---------|---|---|
| a | $4, \frac{1}{2}(6 + \sqrt{6}\lambda)$ | Unstable node $\forall \lambda$ |
| b | $4, \frac{1}{2}(6 - \sqrt{6}\lambda)$ | Unstable node for $\lambda < \sqrt{6}$ Saddle for $\lambda > \sqrt{6}$ |
| c \pm | $-1 \pm \frac{\sqrt{8\lambda^2 - 3\lambda^4}}{\lambda^2}$ | Stable spiral for $\lambda > 2\sqrt{\frac{2}{3}}$ Stable node for $\sqrt{2} < \lambda \leq 2\sqrt{\frac{2}{3}}$ Saddle point for $\lambda < \sqrt{2}$ |
| f \pm | $\frac{1}{2}(-6 + \lambda^2), -2 + \lambda^2$ | Stable node for $\lambda < \sqrt{2}$ Saddle point for $\sqrt{2} < \lambda < \sqrt{6}$ |
| i | -2, 1 | Saddle point $\forall \lambda$ |

In the phase plots of this system, we will no longer discuss the trajectories that end up moving towards the stable points as we have already established them as one of the possible end states of system (5.40). We are more interested in the trajectories that will not move towards $x = 0$ or any of these stable points in the late stages of their evolution. We see this in Figures 5.10a and 5.10b with the curves represented by purple, cyan and dark orange trajectories. These trajectories evolve towards an increase in kinetic and potential energy of the scalar field. As this behavior is not really clear on the plot of $\lambda = 3$, we show a larger phase space in Figure 5.11.

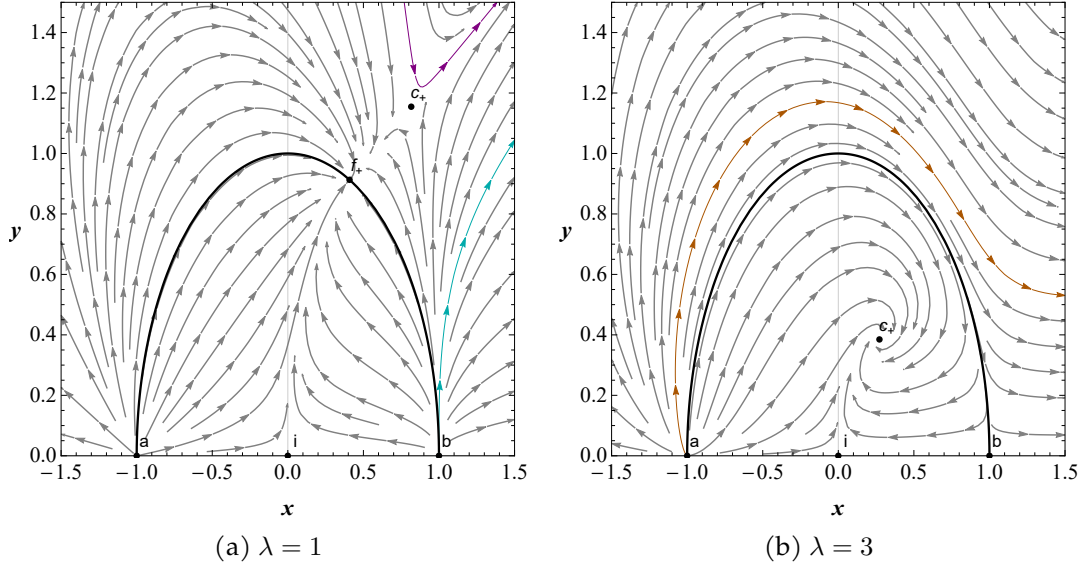


Figure 5.10: Phase plots of system (5.46). The solid black curve represents $x^2+y^2 = 1$.

We also include the temporal evolution of the dark orange trajectory in Figure 5.12 to supplement our analysis with time information. These curves serve as an example for the temporal evolution of trajectories that exhibit increasing kinetic and potential energy of the scalar field in late times. Note that w_{tot} is now equal to w_ϕ with $s = 0$. We see that there is an increase in Ω_ϕ and a decrease in Ω_K which is as expected. This shows that in the absence of dark matter, positively curved universes represented by trajectories with increasing x and y in the late stages of their evolution exhibit a continuous increase in the abundance of dynamic dark energy. Before we move on, notice that our curves get cut off near the e -folding of 1.5 even when there is no discontinuity in the dynamical system. When we look at the full evolution of Ω_ϕ and Ω_K in Figure 5.13, we see that these parameters reach very large values very rapidly so the cut off probably indicates a limit in the numerical integration.

Analog to a mechanical system

There is another interesting analysis to be made for this plane in terms of mechanical systems. Before we discuss this, however, we should first introduce a special case of the system in Eq. (5.46) where H becomes a constant term. For this scenario, notice that Eq. (3.11) becomes zero which turns the said dynamical

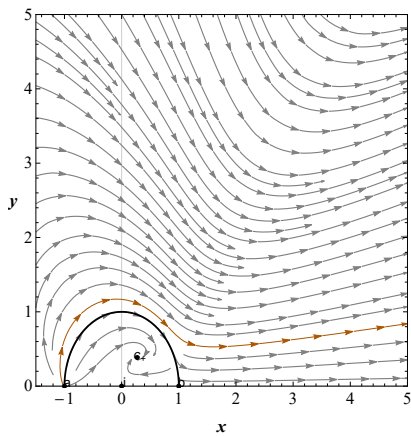


Figure 5.11: A larger phase space of Figure 5.10b

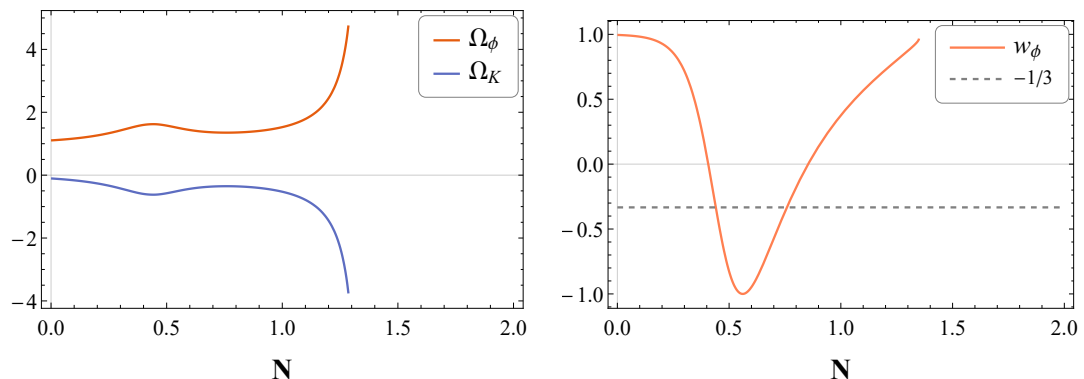


Figure 5.12: Evolution of cosmological parameters Ω_ϕ , Ω_K and w_ϕ with respect to N for the dark brown trajectory in Figure 5.10b

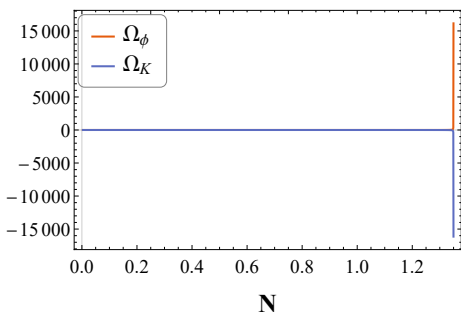


Figure 5.13: The full evolution of Ω_ϕ and Ω_K in Figure 5.12a

system into Eq. (5.47)

$$\begin{cases} x' = \sqrt{\frac{3}{2}}\lambda y^2 - 3x \\ y' = -\sqrt{\frac{3}{2}}\lambda yx \end{cases} \quad (5.47)$$

This system has one fixed point at $(x^*, y^*) = (0, 0)$ with corresponding eigenvalues of -3 and 0 calculated from its Jacobian matrix written as

$$J(x^*, y^*) = \begin{pmatrix} -3 & \sqrt{6}y^* \\ -\sqrt{\frac{3}{2}}y^* & -\sqrt{\frac{3}{2}}x^* \end{pmatrix} \quad (5.48)$$

Since one eigenvalue is zero, we must look into the phase plot to determine this point's stability where we find to be an attracting fixed line along the y -axis when $\lambda = 0$ and a stable node otherwise.

Now, let us recall Eq. (5.21) which is the temporal equation of evolution for the scalar field. With the non-existent interaction term Q , this equation is analogous to the motion of a particle in 1D with mass m and displacement x that is affected by a frictional or damping term and by the force due to the potential $V(x)$. This is expressed as

$$\ddot{x} = -\frac{1}{m} \frac{dV(x)}{dx} - \frac{\alpha}{m} \dot{x} \quad (5.49)$$

which is applicable when this force is conservative (*i.e.* the total work done to move it between two points is path-independent) in which $F(x) = -dV(x)/dx$. With α as a constant, Eq. (5.49) physically translates to a situation where any motion of the particle with potential $V(x)$ is counteracted by friction due to $-(\alpha/m)\dot{x}$. Thus, we can say that $-3H\dot{\phi}$ is somewhat like a friction term on the scalar field. Note that we can usually picture the state of kinetic and potential energies of such a particle as a ball rolling around the given potential. Considering the similarities to this mechanical system, this state should be reflected into the behavior of the system in the considered invariant manifold which we can observe using phase plots.

Let us consider sample values of λ . For the constant H case as shown in Figures 5.15a, 5.15b and 5.15c, any initial kinetic component eventually disappears when $\lambda = 0$ as the potential stays the same while an initial negative kinetic component with some potential when $\lambda > 0$ would first have an increase in its kinetic and potential values before vanishing. Noting that we have an exponential potential and applying the rolling ball analogy as shown in Figure 5.14, this is the expected

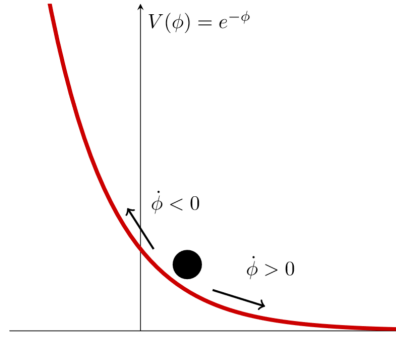


Figure 5.14: The rolling ball analogy for an exponential potential

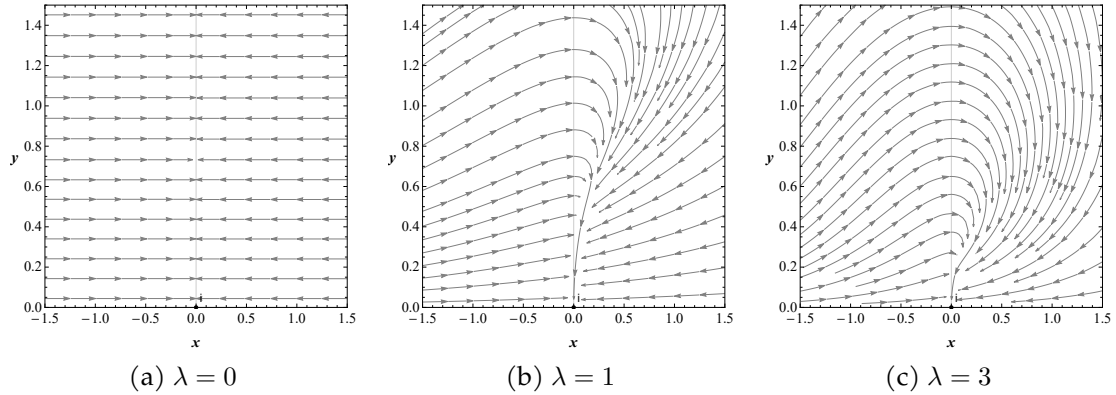


Figure 5.15: Phase plots of system (5.47)

behaviour as the potential becomes flat on a value that is determined by V_0 when $\lambda = 0$. The friction term $-3H\dot{\phi}$ decreases the speed (*i.e.* the kinetic component) of the ball until it stops. On the other hand, negative kinetic values when $\lambda > 0$ mean that the ball would roll up the potential before rolling down and stopping due to the said friction term. However, this is not what we see in the time-varying Hubble parameter case as shown in Figures 5.10a and 5.10b because a time-varying $H(t)$ makes Eq. (5.21) non-autonomous. We can no longer say that $-3H\dot{\phi}$ is like a friction term so the time-varying $H(t)$ cannot be analogous to the discussed mechanical system.

Chapter 6

Conclusions and Recommendations

In our attempt to explore and study the late-time dynamics of a cosmological model that simulates a universe with interacting dark matter and dynamic dark energy, we have tackled concepts behind homogeneous and isotropic universes and the method of dynamical systems. We have also reviewed a model of interacting dark matter and non-dynamic dark energy previously studied by Perez et. al. [20] to be a hands-on example in the application of these concepts.

Although our discussions of the model that is the focus of this thesis are limited to the considered $\{\lambda, \epsilon\}$ parameter space and in the sample phase plots and trajectories that we were able to analyze, we can conclude that a universe with interacting non-zero dark matter and dynamic dark energy would most likely end up as a universe with a cosmological constant as its dark energy. This is because most trajectories end up moving towards the $x = 0$ plane even with the different combinations of fixed points with their corresponding stability we have seen from our phase plots. We have also learned that the presence of stable fixed points leads to special end states. In these special cases, the said universe may end up in various fixed points labeled by $C_{\pm}, D_{\pm}, E_{\pm}, F_{\pm}, G_{\pm}$, or H_{\pm} which represent universes of various curvature with varying proportions of dark matter and dynamic dark energy. In the absence of dark matter, we find that this kind of universe with a positive curvature may not evolve towards the previously mentioned end states but towards an end state of infinitely increasing dynamic dark energy. In addition, we have also learned that the behavior of the said universe with no dark matter component can be analogous to a mechanical system as long as the Hubble parameter is constant.

As possible future works on this topic, we can try out different interaction terms and potentials to see if these would change the end states of this system. We can also

look for an appropriate variable change that will remove the discontinuity in the $x = 0$ plane. Furthermore, we can look for possible mechanical systems that might be analogous to the time-varying $H(t)$ case in the invariant manifold of $s = 0$.

Appendix A

A check for errors in the derivation of system (5.40)

We start with the evolution equation of $\dot{\phi}$ in Eq. (5.21),

$$\ddot{\phi} = -\frac{dV(\phi)}{d\phi} - 3H\dot{\phi} - \frac{Q}{\dot{\phi}} \quad (\text{A.1})$$

Substituting in Eq. (5.25), we have

$$\frac{d\dot{\phi}}{dt} = \kappa\lambda V(\phi) - 3H\dot{\phi} - \frac{Q}{\dot{\phi}} \quad (\text{A.2})$$

Applying the change of variables introduced Eq. (5.5),

$$\frac{d}{dt} \left(\frac{\sqrt{6}H}{\kappa} x \right) = \kappa\lambda \frac{3H^2}{\kappa^2} y^2 - 3H \frac{\sqrt{6}H}{\kappa} x - \frac{\kappa}{\sqrt{6}Hx} Q \quad (\text{A.3})$$

Arranging this, we have

$$\begin{aligned} \frac{d}{dt} (Hx) &= \frac{\kappa}{\sqrt{6}} \kappa\lambda \frac{3H^2}{\kappa^2} y^2 - \frac{\kappa}{\sqrt{6}} 3H \frac{\sqrt{6}H}{\kappa} x - \frac{\kappa}{\sqrt{6}} \frac{\kappa}{\sqrt{6}Hx} Q \\ H\dot{x} + x\dot{H} &= \frac{3}{\sqrt{6}} H^2 \lambda y^2 - 3H^2 x - \frac{\kappa^2}{6Hx} Q \end{aligned} \quad (\text{A.4})$$

after using product rule and cancelling out like terms. Dividing by H^2 , we get

$$\frac{\dot{x}}{H} + x \frac{\dot{H}}{H^2} = \sqrt{\frac{3 \cdot 3}{2 \cdot 3}} \lambda y^2 - 3x - \frac{\kappa^2}{6H^3x} Q \quad (\text{A.5})$$

We isolate \dot{x}/H and apply Eq. (3.17) to obtain

$$\frac{\dot{x}}{H} = x' = \sqrt{\frac{3}{2}} \lambda y^2 - 3x - x \frac{\dot{H}}{H^2} - \frac{\kappa^2}{6H^3x} Q \quad (\text{A.6})$$

Substituting in Eqs. (3.11) and (5.13), we have

$$x' = \sqrt{\frac{3}{2}}\lambda y^2 - 3x + x(1+q) - \frac{\kappa^2}{6H^3x} \frac{3H^3}{\kappa^2} \epsilon [x^2 + y^2] s^2 \quad (\text{A.7})$$

Thus,

$$x' = \sqrt{\frac{3}{2}}\lambda y^2 - 3x + x(1+q) - \frac{1}{2x}\epsilon [x^2 + y^2] s^2 \quad (\text{A.8})$$

which is the same as the x' obtained in Chapter 5. Therefore, we can infer that our equation for x' is correct. As for y' , we can use Ω'_ϕ and its relation with x and y given by (5.6). Note that

$$\begin{aligned} \Omega'_\phi &= \frac{d(x^2 + y^2)}{dN} \\ &= \frac{d(x^2 + y^2)}{dx} \frac{dx}{dN} + \frac{d(x^2 + y^2)}{dy} \frac{dy}{dN} \\ \Omega'_\phi &= 2xx' + 2yy' \end{aligned} \quad (\text{A.9})$$

As mentioned before, we apply a change of variables to the system in Eq. (4.30). To indicate this change, we recast Ω_{de} to Ω_ϕ . Then, the prime derivative of Ω_ϕ

$$\Omega'_\phi = \Omega_\phi[-1 - 3w_\phi + (1 + 3w_\phi)\Omega_\phi + (1 - \epsilon)\Omega_{\text{dm}}] \quad (\text{A.10})$$

becomes

$$\begin{aligned} 2xx' + 2yy' &= (x^2 + y^2) \left[-1 - 3\frac{x^2 - y^2}{x^2 + y^2} + \left(1 + 3\frac{x^2 - y^2}{x^2 + y^2} \right) (x^2 + y^2) + (1 - \epsilon)s^2 \right] \\ &= (x^2 + y^2) \left[-1 - 3\frac{x^2 - y^2}{x^2 + y^2} + (x^2 + y^2 + 3x^2 - 3y^2) + s^2 - \epsilon s^2 \right] \\ &= (x^2 + y^2) \left[-1 - 3\frac{x^2 - y^2}{x^2 + y^2} + (4x^2 - 2y^2 + s^2) - \epsilon s^2 \right] \\ &= -(x^2 + y^2) - 3(x^2 - y^2) + 2q(x^2 + y^2) - \epsilon(x^2 + y^2)s^2 \\ 2xx' + 2yy' &= -4x^2 + 2y^2 + 2q(x^2 + y^2) - \epsilon(x^2 + y^2)s^2 \end{aligned} \quad (\text{A.11})$$

Isolating yy' ,

$$yy' = -2x^2 + y^2 + q(x^2 + y^2) - \frac{1}{2}\epsilon(x^2 + y^2)s^2 - xx' \quad (\text{A.12})$$

Substituting in x' that we obtained from $\ddot{\phi}$, we obtain

$$\begin{aligned} yy' &= -2x^2 + y^2 + q(x^2 + y^2) - \frac{1}{2}\epsilon(x^2 + y^2)s^2 - \sqrt{\frac{3}{2}}\lambda y^2 x + \\ &\quad 3x^2 - x^2(1+q) + \frac{1}{2}\epsilon[x^2 + y^2]s^2 \end{aligned} \quad (\text{A.13})$$

which leads to

$$\begin{aligned} yy' &= y^2 + qx^2 + qy^2 + x^2 - \sqrt{\frac{3}{2}}\lambda y^2 x - x^2(1+q) \\ &= \cancel{x^2(1+q)} + y^2(1+q) - \sqrt{\frac{3}{2}}\lambda y^2 x - \cancel{x^2(1+q)} \end{aligned} \quad (\text{A.14})$$

after cancelling like terms. Finally, dividing both sides by $\frac{1}{y}$ gives

$$y' = -\sqrt{\frac{3}{2}}\lambda yx + y(1+q) \quad (\text{A.15})$$

In the same manner, we can use Ω'_{dm} for calculating s' . Note that

$$\Omega'_{\text{dm}} = \frac{d(s^2)}{dN} = \frac{ds^2}{ds} \frac{ds}{dN} = 2ss' \quad (\text{A.16})$$

Thus, Ω'_{dm} given in (4.30)

$$\Omega'_{\text{dm}} = \Omega_{\text{dm}} [-1 + (1 + 3w_\phi + \epsilon)\Omega_\phi + \Omega_{\text{dm}}] \quad (\text{A.17})$$

becomes

$$\begin{aligned} 2ss' &= s^2 \left[-1 + \left(1 + 3\frac{x^2 - y^2}{x^2 + y^2} + \epsilon \right) (x^2 + y^2) + s^2 \right] \\ &= s^2 \left[-1 + x^2 + y^2 + 3x^2 - 3y^2 + \epsilon(x^2 + y^2) + s^2 \right] \\ &= s^2 \left[-1 + 4x^2 - 2y^2 + s^2 + \epsilon(x^2 + y^2) \right] \\ 2ss' &= s^2 \left[-1 + 2q + \epsilon(x^2 + y^2) \right] \end{aligned} \quad (\text{A.18})$$

Isolating s' and arranging the resulting equation gives

$$s' = s \left[\frac{1}{2}\epsilon(x^2 + y^2) - \frac{1}{2} + q \right] \quad (\text{A.19})$$

Since the form of y' and s' are equivalent to those that were obtained before, their formulation must be correct as well.

Bibliography

- [1] Heinz Andernach and Fritz Zwicky. English and spanish translation of zwicky's (1933) the redshift of extragalactic nebulae. 2017.
- [2] A. S. Arapoglu and A. E. Yükselci. Dynamical System Analysis of Quintessence Models with Exponential Potential - Revisited. *Modern Physics Letters A*, 11 2017.
- [3] E. Aydiner. Chaotic universe model. *Sci Rep*, 8(721), 2018.
- [4] C. Boehmer, G. Caldera-Cabral, N. Chan, R. Lazkoz, and R. Maartens. Quintessence with quadratic coupling to dark matter. *Phys. Rev. D*, 81, 11 2009.
- [5] N. Böhmer, C. and Chan. Dynamical Systems in Cosmology. *Dynamical and Complex Systems*, page 121–156, Dec 2016.
- [6] G. Caldera-Cabral, R. Maartens, and L.A. Ureña-López. Dynamics of interacting dark energy. *Phys. Rev. D*, 79(6), Mar 2009.
- [7] S. Carroll. *Spacetime and Geometry: An Introduction in General Relativity*. Addison-Wesley, 2004.
- [8] P. H. Chavanis. Cosmology with a stiff matter era. *Physical Rev. D*, 92, 11 2014.
- [9] D. Clowe, M. Bradač, A. H. Gonzalez, M. Markevitch, S. W. Randall, C. Jones, and D. Zaritsky. A direct empirical proof of the existence of dark matter. *The Astrophysical Journal*, 648(2):L109–L113, Aug 2006.
- [10] D. Clowe, A. Gonzalez, and M. Markevitch. Weak-lensing mass reconstruction of the interacting cluster 1e 0657-558: Direct evidence for the existence of dark matter. *Astrophysical Journal - ASTROPHYS J*, 604:596–603, 04 2004.

- [11] N. Deruelle and J Uzan. *Relativity in Modern Physics*. Oxford University Press, 2018.
- [12] Gerson Goldhaber and David B. Cline. The acceleration of the expansion of the universe: A brief early history of the supernova cosmology project (scp). *AIP Conference Proceedings*, 2009.
- [13] J. Hofbauer and K. Sigmund. *Evolutionary Games and Population Dynamics*. Cambridge University Press, 1998.
- [14] F. Hoppensteadt. Predator-prey model. *Scholarpedia*, 1(10):1563, 2006. revision #91667.
- [15] E. M. Izhikevich. Equilibrium. *Scholarpedia*, 2(10):2014, 2007.
- [16] H. Kragh. *Conceptions of Cosmos: From Myths to the Accelerating Universe: A History of Cosmology*. Oxford University Press, 2007.
- [17] Amendola L. and Tsujikawa S. *Dark Energy: Theory and Observations*. Cambridge University Press, 2010.
- [18] K. Nozari, N. Behrouz, and N. Rashidi. Interaction between Dark Matter and Dark Energy and the Cosmological Coincidence Problem. *Adv. High Energy Phys.*, 2014:569702, 2014.
- [19] A. Paliathanasis, S. Pan, and W. Yang. Dynamics of nonlinear interacting dark energy models. 2019.
- [20] J. Perez, A. Fuzfa, T. Carletti, L. Melot, and L. Guedezounme. The Jungle Universe: Coupled cosmological models in a Lotka-Volterra framework. *General Relativity and Gravitation*, 6, 06 2014.
- [21] L. E. Persson. A basic course in applied mathematics. *Applied Mathematics, Lecture notes, Luleå University of Technology, Sweden*.
- [22] Adam G. Riess, Alexei V. Filippenko, Peter Challis, Alejandro Clocchiatti, Alan Diercks, Peter M. Garnavich, Ron L. Gilliland, Craig J. Hogan, Saurabh Jha, Robert P. Kirshner, and et al. Observational evidence from supernovae for an accelerating universe and a cosmological constant. *The Astronomical Journal*, 116(3):1009–1038, Sep 1998.

- [23] M. Roussel. Stability analysis for ODEs. *Nonlinear Dynamics, Lecture notes, University Hall, Canada*, 2005.
- [24] N. Roy and N. Banerjee. Quintessence Scalar Field: A Dynamical Systems Study. *The European Physical Journal Plus*, 129, 02 2014.
- [25] V. C. Rubin, W. K. Ford, Jr., N. Thonnard, and D. Burstein. Rotational properties of 23sb galaxies. *Astrophysical Journal - ASTROPHYS J*, 261:439–456, 10 1982.
- [26] B. Ryden. *Introduction to Cosmology*. Pearson Education, Inc., second edition, 2017.
- [27] A. Serra and M. Dominguez. Measuring the dark matter equation of state. *Monthly Notices of the Royal Astronomical Society*, 415, 03 2011.
- [28] S. Strogatz. *Nonlinear Dynamics and Chaos: With Applications to Physics, Biology, Chemistry, and Engineering*. Westview Press, 2015.
- [29] J. Uzan and R. Lehoucq. A Dynamical Study of the Friedmann Equations. *European Journal of Physics*, 22, 08 2001.
- [30] J. Wainwright and G.F.R. Ellis. *Dynamical Systems in Cosmology*. Cambridge University Press, 1997.
- [31] S. Watson. An Exposition on Inflationary Cosmology. April 2000.
- [32] S. Weinberg. The cosmological constant problem. *Rev. Mod. Phys.*, 61:1–23, Jan 1989.
- [33] I. Zlatev, L. Wang, and P. Steinhardt. Quintessence, Cosmic Coincidence, and the Cosmological Constant. *Phys. Rev. Lett.*, 82:896–899, Feb 1999.